SLAC–PUB–6032
November 1993
(A)

DESIGN AND SIMULATION OF ACCELERATING STRUCTURES FOR FUTURE LINEAR COLLIDERS*

K.A. Thompson, C. Adolphsen, K.L.F. Bane,

H. Deruyter, Z.D. Farkas, H.A. Hoag, K. Ko,

G.A. Loew, R.H. Miller, E.M. Nelson, R.B. Palmer,

J.M. Paterson, R.D. Ruth, J.W. Wang, P.B. Wilson,

Stanford Linear Accelerator Center, Stanford University, Stanford, California 94309

N.M. Kroll, X.T. Lin

Physics Department, University of California, San Diego, La Jolla, California 92093

R.L. Gluckstern

Physics Department, University of Maryland, College Park, Maryland 20742

N. Holtkamp

DESY, Notkestrasse 85, D-22603 Hamburg 52, Germany

B.W. Littmann

Institut für Theoretische Elektrotechnik, TU Berlin, D-10587 Berlin, Germany

D.U.L. Yu

DULY Research Inc., Rancho Palos Verdes, California 90732

Submitted to *Particle Accelerators*

⋆ Work supported by the Department of Energy, contract DE-AC03-76SF00515, and DOE SBIR grants DE-AC03-87ER80529 and DE-FG03-90ER81080.

ABSTRACT

In order to obtain high luminosity and energy efficiency in future linear colliders, it is desirable to accelerate a train of closely spaced bunches on each rf pulse of the machine. There can be severe multibunch beam break-up in such a collider unless some means of strongly suppressing the transverse wakefield is incorporated into the design of the accelerating structures. Two methods of wakefield suppression will be discussed in this paper: (1) damping, i.e., lowering the external Q's of the unwanted higher-order modes induced by the beam in the cells of the accelerating structures, and (2) detuning, i.e., varying the frequencies of the higher-order modes (by varying the cell and iris radii along the structure) so that the net induced wakefield rapidly decoheres. The design and simulation of damped and detuned structures will be discussed. Beam dynamics simulations incorporating an accelerating structure design for the SLAC Next Linear Colider (NLC) are presented.

1. Introduction

1.1 Motivation for multibunching and wakefield suppression

Two critical requirements that must be met in the design of future e^+e^- linear colliders are high luminosity and efficient use of the rf power available in the accelerating structures. The luminosity required by high-energy physics experiments at an e^+e- collider with center-of-mass energy of about 0.5 to 1 TeV is in the range 10^{33} to 10^{34} $\mathrm{cm}^{-2}\mathrm{sec}^{-1}$. There are at present several approaches to the design of such a next-generation linear collider [1-4]. Most of these designs utilize multibunching, i.e., the acceleration of a train of bunches rather than just a single bunch on each rf fill of the accelerating structures. The major motivation for multibunching is to maximize the luminosity for a given average rf power.

Several of the designs for a future linear collider, including the Next Linear Collider (NLC) design being pursued at Stanford Linear Accelerator Center (SLAC), are based upon extensions of conventional rf technology to the X-band frequency range, above 10 GHz. One reason for departing from the conventional S-band ($\sim$ 3 GHz) frequency is to reduce the power requirements. However, even at X-band the power requirements are high, and it is desirable to extract as much of the available rf energy as possible. Another reason for going to X-band is the possibility of obtaining higher accelerating gradients (50 to 100 MV per meter), thus reducing the length and cost of the main linacs.

An essential problem that must be addressed in these smaller structures, however, is their relatively higher wakefields. The passage of rather intense, closely-spaced bunches through an accelerating structure produces both transverse and longitudinal wakefields that influence the orbits and energies of subsequent bunches. In a conventional disk-loaded structure, these wakefields would ring for many multiples of the required bunch separation. If the transverse wake is not suppressed, the cumulative beam break-up instability is extremely severe, leading to emittance blow-up and eventual loss of the beam. Thus, the main problem is to obtain adequate suppression of the transverse wakefield, which is the subject of this paper.

The electric field pattern of the most damaging transverse dipole mode is shown in Fig. 1.

Although it is not the subject of this paper, the longitudinal wake, responsible for beam-loading in the accelerating structures, must also be dealt with. Significant beam-loading at the accelerating frequency is unavoidable, but may be compensated by various means. One method, well-suited to short bunch trains, is to introduce the bunch train before a given accelerating structure is completely filled, thus allowing the additional filling of the structure during the time between successive bunches to approximately compensate for the energy extracted by each bunch [5]. For the longer bunch trains (of order a filling time in length) presently under consideration for the NLC, shaping of the input rf pulse is a useful strategy [6,7,8]. However, one must also make sure that beam-loading in the higher-order modes of the longitudinal wake is sufficiently suppressed that it does not upset the energy compensation produced by such schemes. Preliminary work indicates that our methods of suppressing the transverse wake will also sufficiently suppress the higher-order longitudinal modes.

1.2 Methods of wakefield suppression

Two general methods of suppressing the transverse wake fields have been studied. The first is to damp the unwanted higher-order modes (HOMs), i.e., to lower their external Qs. The second is to detune the modes, i.e., to design an rf accelerating structure in which the frequencies of corresponding HOMs differ sufficiently from cell to cell that the wake decoheres rapidly.

Wake field suppression for the 10 to 20 bunch design initially proposed for the NLC could in principle be achieved either by strong damping alone or by detuning alone. However, the present NLC design calls for a longer bunch train. This choice is a result of optimizing the design to maximize luminosity, minimize backgrounds, and ease certain other technical considerations. For example, the requirement on the bunch aspect ratio (Refs. 1–4). If detuning is used as the main method of

suppressing the wake, one must ensure that the wake does not recohere significantly during the passage of the longer bunch train. Thus it may be necessary to take additional measures to control the long-range wake.

One possibility is to combine the two cures mentioned so far [9], that is, to use detuning to produce a rapid initial roll-off of the wakefield, and use a moderate amount of damping to suppress it at longer distances. It is, however, probably necessary to moderately damp many cells in the structure, which may not be significantly easier than strongly damping all cells.

Another possible means of suppressing the longer-range wake is to vary the distribution of HOM frequencies from structure to structure (instead of, or in addition to, varying them within the structures). Such section-to-section frequency variation has been proposed as the main method of wakefield suppression in some S-band linear collider designs [10]. We have proposed a particular form of section-to-section variation as a possible adjunct to intrasection detuning in the NLC X-band design [11]. In this scheme, the set of frequencies in several different structure types are interleaved so that, in effect, one has a smoother and denser distribution of frequencies than with just one structure type. This leads to much-improved suppression of the longer-range wake behavior.

1.3 Historical perspective

The ideas of damping and detuning unwanted HOMs both have roots prior to the era of linear colliders. Damping antennas incorporating ferrites to absorb HOMs in standing-wave accelerating cavities have been in use for a number of years. Damping of HOMs by coupling the power out of the cavity through appropriately designed waveguides was first suggested by Palmer [12], and will be discussed further in the next section.

Detuning in linacs has a somewhat more involved history. Detuning is present in the existing SLAC linac because of the constant-gradient design of the structure.

It was not originally introduced for the purpose of suppressing the transverse wakefield. When the SLAC linac was turned on in 1966, a new multibunch transverse instability was discovered [13]. It was quickly realized that this instability was due to the excitation of transverse dipole deflecting fields by a beam with transverse offsets in a series of accelerating structures [14]. In effect, the linear accelerator acted as an amplifier for the transverse noise modulation of the beam at frequencies in the neighborhood of 4.14 GHz.

A similar effect involving the same dipole modes had previously been seen in single-section accelerators running at high peak currents ($\sim$ 1A), in which the accelerator behaved as a backward wave oscillator excited by transverse noise on the beam. The SLAC linac ran at currents well below the threshold for this single-section instability, known as *regenerative* beam break-up. The new instability, which came to be denoted *cumulative* beam break-up, arose because a small amplification in each successive section of the SLAC linac (consisting of about 960 nominally identical sections) created a large total amplification ($\sim 10^6$ or 10^7).

The amplification would have been disastrously higher were it not for the fact that the sections of the SLAC linac were designed to be "constant-gradient", i.e, the accelerating structure is tapered to maintain a constant accelerating electric field even though the power flowing through the structure is attenuated between the input and the output ends. This was accomplished [15] by decreasing the size of the coupling irises between cells in order to decrease the group velocity linearly with distance along each section. The diameter of each cell was adjusted in the design to keep the phase velocity equal to the velocity of light. An unplanned benefit was that the dipole modes of the SLAC structure were detuned. This occurred because reducing the iris size lowered the frequency of the accelerator mode (TM_{01}) of each cell, but raised the frequency of the dipole modes (TM_{11} and TE_{11} hybrids). Adjusting the cell diameter to keep the frequency of the accelerating mode constant detuned the dipole modes even further. In the SLAC structures this produced a total frequency spread of the dangerous dipole modes of about 5%. The net effect of this detuning was that the dipole modes acted coherently only over a length of

about 30 cm at the beginning of the structure, reducing the effective dipole mode impedance by an order of magnitude.

Without this unintentional detuning, the beam break-up (BBU) threshold at SLAC (the current at which the beam gets scraped at the end of the 1.6 μs pulse) would have been 1 or 2 mA instead of 15 mA. In order to raise the BBU threshold beyond the design current of 50 mA, two corrective measures were taken [16]:

1. The strength of the focusing was roughly tripled by redistributing the quadrupoles, which were originally placed in triplets at 100 meter spacing. At full machine energy, the new arrangement had a betatron wavelength $\lambda_\beta \approx 150$ m in the first 600 meters of the linac, $\lambda_\beta \approx 400$ m for the next 1800 meters, and constant quadrupole strength for the remainder of the machine. This program approximately doubled the BBU threshold.

2. The highest impedance dipole modes, which were trapped at the input end of the structure, were detuned. The 960 accelerator sections were divided into three equal groups. The detuning was done by dimpling the 2nd, 3rd and 4th cells of the structures to be detuned, so as to change the resonant frequency of the dipole mode by 2 MHz in 1/3 of the structures, and by 4 MHz in 1/3 of the structures, with 1/3 remaining as built. The detuning was done *in situ*, cost less than 1% in beam energy, and gained another factor of 2.5 in beam current.

A number of multisection high duty factor electron linear accelerators have since incorporated detuning to suppress cumulative beam breakup [17]. In these accelerators a much more aggressive detuning was possible since it was part of the initial design.

1.4 Application of detuning to future linear colliders

Given the experience with the original SLAC linac, it was natural to consider exploiting detuning in the design of the NLC. At first, a small amount of detuning (2–4%), with a uniform distribution of frequencies, was investigated as a possible adjunct to damping [18,19] but this small spread was not enough to have a very significant effect. Another idea, the beating of two or more different HOM frequencies with dipole frequency spread about 10% in order to produce beat minima near which NLC bunches could be placed was also investigated at around the same time [20].

Detuning in the NLC became more promising when it was realized that considerably larger detuning spreads might be feasible and that shaping the density profile of the distribution was another factor that could be used to advantage [21]. With the structure parameters chosen at SLAC for the NLC, a constant-gradient structure design would spread the dipole mode frequencies by about 10%. The first calculation was done for a uniform distribution of wakefield resonances with a full spread of 10%; for this case, the envelope of the wakefield amplitude in time is a $\sin x/x$ distribution. This suggested that a Gaussian density distribution of the dipole resonances might be close to ideal. With 200 cells in a (truncated) Gaussian frequency density distribution, the wakefield drops after about 20 cycles to a level somewhat less than that of a single cell and stays at that level for several hundred cycles. The more cells included in the Gaussian density distribution, the longer the integrated amplitude remains small. This improvement of the suppression is limited by the fabrication tolerances and by the fact that when the length of a structure (or series of structures) is comparable to the Twiss parameter β of the focusing lattice, it is no longer valid to simply add the wakefields from all the cells. Detailed tracking calculations must be made, including kicks from both the dipole wakefield modes and the focusing lattice, at their proper locations.

This method of detuning was soon examined in more detail by several authors [9,22,23]. The main focus has been on suppressing the effect of the lowest frequency

transverse HOM, since its kick factor is greater than those of the higher transverse HOMs by about an order of magnitude. Furthermore, the sum of the higher frequency HOMs will tend to decohere more rapidly and become even less important at long distances. Nevertheless, it is necessary to ensure that all the HOMs, both transverse and longitudinal, are sufficiently well suppressed to meet the stringent beam energy and emittance tolerances. An approach to decohering these other higher frequency modes by varying the iris thicknesses along the detuned structure is being pursued at SLAC [24], and preliminary results indicate that the HOM's can indeed be controlled in this fashion.

1.5 NLC PARAMETERS

Table 1: Parameters for NLC main linacs	
rf frequency	11.424 GHz
Initial average beta function	4.0 m
Initial linac energy	18 GeV
Final linac energy	250 GeV 500 GeV (upgrade)
Linac active length	6000 m
Particles per bunch	1×10^{10}
Bunch spacing	1.4 nsec

The NLC design parameters used in this paper are shown in Table 1. The value of about 1.4 nsec (16 rf wavelengths) for the bunch spacing is the minimum being considered.

Note that with the given initial energy, final energy, and active length (total length of rf structures) per linac, the average loaded accelerating gradient is a little less than 40 MeV/m. The gradient for a possible high-energy upgrade would be

about twice as much, but for the present examples we shall use the lower energy since this leads to greater blowup of the beam from the wakefield kicks. The value of the bunch charge in an optimized design may be somewhat less than the conservative value of 1×10^{10} used here.

The average beta function is 4.0 m at the beginning of the linac, and it will be assumed to increase approximately as the square root of the energy:

$$\beta \approx \left(\frac{\gamma}{\gamma_0}\right)^{1/2} \beta_0 \quad , \tag{1.1}$$

where $\gamma = E/m_0c^2$, and E and m_0 are the electron total energy and rest mass, respectively.

The length of the bunch train is still under consideration. One case that has been under study for some time is a "short pulse" design, having about 10 bunches per train and extracting around 25% of the available rf energy. More recently, the train length under consideration has gone up to 90 or more bunches, which gives a train length greater than the filling time ($\sim$ 100 ns); in this case the efficiency of extraction of rf energy can be higher, provided that rf pulses of suitable length and shape can be produced.

1.6 Scope of paper

In the remainder of this paper we discuss the calculation of wakefields in damped and detuned structures, and we discuss the simulation of the effect of these wakefields on the beam. Considerable effort has gone into accurately calculating the Qs of the most important wake field modes in various configurations of damped cavities. Some of this work has already been documented in the literature; a brief summary and update are given in the next section. Next we discuss the simulation of wake fields in detuned structures. In this case, we have developed and applied suitable equivalent circuit models, since direct calculations using programs such as TBCI [25] are impractical from the standpoint of meshing and CPU requirements.

Finally, beam dynamics calculations, including simulations illustrating the control of beam break-up achieved in an NLC design, are presented.

2. Design and simulation of damped structures

As discussed in the introduction, one way to suppress the long range wakefield is to heavily damp the HOMs of the accelerator cavities. In order for such an approach to be of practical interest, the damping must be done in such a way as to minimize the degradation of the accelerating mode shunt impedance r, the r/Q, and the symmetry of the rf field pattern. A general approach to achieving this was proposed in Ref. 12, the basic idea being to strongly couple unwanted modes of the accelerator cavity cells to matched load-terminated waveguides. To damp the HOMs without damping the accelerating mode, one can either choose a geometry in which the waveguides are cut off at the accelerating mode frequency but not at the frequencies of the HOMs to be damped [26], or a geometry in which the accelerating mode is decoupled from the waveguide even though the cutoff frequency of the waveguide is below that of the accelerating mode [27]. Two generic coupling schemes were proposed:

1. A configuration in which rectangular TE_{10} mode waveguides are coupled to radial slots in the loading disks. This will be referred to as "radial-slot" coupling.

2. A configuration in which rectangular TE_{10} mode waveguides (polarized orthogonally to those proposed for the "radial-slot" case) are coupled through circumferential slots to the side walls of the accelerator cavity cells. This will be referred to as "circumferential-slot" coupling,

An example of the radial-slot configuration is shown in Fig. 2. An example of the circumferential-slot configuration, a "crossed waveguide" structure, is shown in Fig. 3. Preliminary measurements reported in Ref. 12 indicate that it is likely that at least the radial-slot configuration can produce adequate damping. Var-

ious implementations of the circumferential-slot configuration were subsequently investigated as well and were also found capable of producing strong damping.

2.1 Radial-slot configuration

Because the preliminary measurements suggested that radial-slot damping was the more effective method, initial experimental investigation was directed at this configuration. A four-fold symmetry was suggested in Ref. 12. Such a configuration preserves accelerating mode symmetry reasonably well and provides damping for both dipole mode orientations. In order to also provide some damping for both quadrupole mode orientations, it was proposed to rotate the symmetry axes by 45 degrees from cell to cell. This expedient was also suggested by a potential problem with waveguide overlap between successive cavities. Properly designed ridge waveguides, which couple naturally to the radial slots, could, however, also solve the overlap problem. Experiments were performed to investigate fabrication problems; to determine how the quadrant slots affect the fundamental and HOM frequencies, field patterns, and rf voltage breakdown limits; and to investigate the damping of the HOMs [21,28,29].

The experimental work was supplemented by MAFIA [30] calculations and a new approach which provides both an experimental and a MAFIA-based method of determining the Qs of the HOMs [27,31]. The method is closely related to a method proposed by Slater [32] and is based upon a study of the modes of the coupled cavity system formed by shorting the damping waveguides at various lengths. Calculations (Ref. 27) were carried out for a model (see Fig. 2) consisting of two coupled accelerator half-cavities damped by ridge waveguides coupled to each of two radial slots in the iris between the two cavities. The ridge thickness is the same as the loading disk thickness, and the ridge gap is same as the width of the slot in the loading disk. A value of 8.7 was found for the Q_{ext} of the dipole π-mode, while the dipole zero-mode and the monopole modes were undamped (neglecting wall losses). Although the cutoff frequency of the ridge waveguide is well below the frequencies of the monopole modes, these modes are undamped

because of a polarization mismatch of the fields. A similar remark applies to the undamped dipole zero-mode. The behavior of the two dipole modes shows that the dipole mode damping obtained with this scheme depends upon the cell-to-cell phase advance, but as the frequency is such that synchronous velocity implies a phase advance close to π, adequate damping can be expected. Low frequency slot modes, the bulk of whose energy resides in the slots in the irises, were also found, but these were even more heavily damped. While coupling to other higher dipole modes has not been investigated in any systematic quantitative way, it is considered to be likely, perhaps with some dimensional modifications, that these can be satisfactorily damped as well. Cold test results (Ref. 29) on models similar to the model analyzed in Ref. 27 lead to the same conclusion. These two-slot models of course damp only one of the two dipole mode orientations, but it is expected, as mentioned above, that four slots would damp them both. We note, however, that the work of Conciauro and Arcioni [33] implies that a three slot configuration would also damp both dipole mode orientations. In this configuration, dipole and quadrupole modes are mixed and are all damped without resorting to cell-to-cell rotations of the slots and waveguides. Because of this advantage it is likely that a three-slot configuration would be used in any practical application.

2.2 Circumferential-slot configuration

Although the radial-slot configuration appears to provide satisfactory damping, fabrication problems were anticipated. It was therefore deemed prudent to investigate the circumferential-slot alternative. Initial configurations studied consisted of accelerator cavities coupled to two or four rectangular waveguides connected directly to the cavity side walls, sometimes with an intervening iris. Ridge waveguides were also studied. It is necessary to choose waveguide dimensions so that the cutoff frequency of the TE_{10} mode is above the frequency of the accelerating mode but below the frequency of any mode one wishes to damp. Because penetration of the fields of the accelerating mode into the waveguides degrades both the Q_0 and the shunt impedance, it is undesirable to have the cutoff frequency

close to the accelerating frequency. The separation of the accelerating and dipole mode frequencies is typically rather small and was found to be made even smaller by the waveguide loading. Indeed a dipole mode which is above the cutoff before the cavity is coupled to the waveguide can fall below cutoff after coupling, thus becoming an undamped mode. Furthermore, even those modes which are above cutoff are poorly damped when too close to cutoff. Thus the choice of parameters is quite constrained. Nevertheless, when all constraints were satisfied, very strong damping was observed for the principal dipole mode in structures with fourfold symmetry, as discussed later in this paper.

In attempting to apply computer simulations to these structures, the damping was found to be so strong that it was difficult, employing the methods of Refs. 27 and 31, to determine Q_{ext} and to separate cavity resonances from waveguide resonances. An improvement in the method was therefore developed. The information obtained from the previously described MAFIA computations can be used to plot the phase of the reflection coefficient from the cavity as a continuous function of frequency [34]. Because cavity resonances are associated with phase changes of $\sim \pi$, the phase versus frequency plots provide a useful way of distinguishing cavity resonances from waveguide resonances and also a way of recognizing the presence of broad overlapping resonances. Methods were developed for determining the parameters of overlapping resonances as well. This approach was applied to the analysis of a waveguide-damped accelerator structure with threefold symmetry [35], and extremely low values were found for Q_{ext} (< 3 for the lowest dipole mode).

As in the case of the radial-slot type of coupling, a systematic study of all potentially threatening higher-order modes was not carried out. As pointed out in Ref. 33, if the waveguides are placed symmetrically between the accelerating irises, the TM_{011} mode is undamped. This is because it does not couple to the TE_{10} waveguide mode and probably always has a frequency below the cutoff of the waveguide modes to which it does couple. A similar problem can occur for other higher-order axial modes such as TM_{01n}. This problem can be dealt with by introducing some axial asymmetry, for instance by introducing an asymmetric iris

or placing the waveguide asymmetrically. Preliminary investigations have indicated that the latter alternative is more satisfactory. A computer simulation of a modified form of the crossed waveguide structure was carried out — the crossed waveguide structure of Fig. 3 was modified by shifting one of the waveguide walls such that the waveguide height was reduced by 36%. The simulation yielded a Q_{ext} of 74 for the TM_{011} mode without significantly compromising the excellent damping of the dipole mode.

Conciauro and Arcioni (Ref. 33) found for a similar configuration a 10% reduction in r/Q and a 10% reduction in the Q of the accelerating mode, results which we believe to be typical of circumferential-slot damping. The degradation of these quantities is expected to be significantly smaller for the radial-slot configuration.

2.3 Some general considerations in damped structures

If wall losses due to finite conductivity are neglected, the decay at large values of time cannot be completely described in terms of exponentially damped modes [36]. This is because energy deposited in an accelerator cavity at or near a waveguide cutoff frequency propagates through the waveguide at zero or small group velocity, leading to persistent wakefields which decay as inverse powers of time t rather than exponentially (the dependence of the leading term for the transverse wakefield is $t^{-3/2}$). While it is obvious that this is the dominant effect at sufficiently large values of t, the question of practical interest is whether it is dominant at times of the order of the duration of a pulse train. Reference 36 discusses wakefields for two structures which are generically similar to the crossed waveguide structure. In both cases the persistent wake dominates at times greater than a typical interval between individual bunches, so that the damped cavity modes are actually less important than the persistent wake for these examples. Irises which reduce the damping also appear to decrease the amplitude of the persistent wake. For a given bunch separation it is likely that there is some optimum level of waveguide damping which minimizes the total wakefield for the relevant time interval. On the basis of the examples studied so far it seems very likely that this minimized level is well

below that which would cause beam instability for the NLC bunch charge and bunch spacing.

The above discussions are based on the assumption that the damping waveguides are terminated by matched loads. The problem of how these loads are to be provided has not been satisfactorily solved at this point and is one of the reasons for our decision to pursue detuning more intensively. One issue is that of absorbing the power coupled out of the central cavity in a very limited radial space, since cost and other considerations make it desirable to minimize the diameter of the complete structure.

3. Design and simulation of detuned structures

Recent work at SLAC has been focused on the exploration of detuning as a means of wakefield suppression. We turn now to a discussion of the theoretical work we have done on this subject.

Intuitive understanding of the effects of detuning is most easily obtained by viewing the structure as consisting of a collection of uncoupled oscillators corresponding to the synchronous modes of the periodic structures one could construct from each of the cells in the structure. The quantitative results of this simple approximation, which we shall refer to as the "uncoupled model", turn out to be quite good, and it will be the first model presented. Then we shall discuss the procedures by which the structure dimensions are obtained from the desired uncoupled frequency distribution, and we evaluate various rf parameters.

A more complete treatment should include the effects of the small couplings between the oscillators; we do this via equivalent-circuit models. A brief summary of two such models (a single-passband model and a model which takes into account the mixing of the two lowest dipole passbands) is given. We then discuss the effects of structure-to-structure variations, where the differences may be introduced deliberately or may be due to finite fabrication tolerances. Finally, we discuss briefly the mechanical design of the detuned structure.

3.1 Uncoupled model for cell-to-cell detuning

As a simple initial model for detuning, let us consider a single transverse deflecting mode. Let the mode have frequency f_1 so that before detuning it gives a wake function

$$W(t) = W_1 \sin(\omega_1 t) \exp(-\omega_1 t/2Q_1) \quad , \tag{3.1}$$

where $\omega_1 = 2\pi f_1$. The wake function $W(t)$ is defined such that, given a charge q travelling at the speed of light and with transverse offset x with respect to the axis of the structure, the average transverse force experienced by a test charge following a time t afterwards is $F_\perp = eW(t)qx$. The wake function in Eq. (3.1) is that for a particular synchronous ($v = c$) mode in a periodic travelling wave structure. The coefficient W_1 has units V/C/m^2 and is equal to twice the transverse kick factor [37] K of the dipole mode in question:

$$K = \frac{c(dE_\perp/dr)^2_{r=0}}{4\omega Up} \quad . \tag{3.2}$$

Here r is directed radially away from the structure axis, U is the stored energy per unit length, p the structure period, a the iris radius, ω the mode frequency, and c the speed of light.

Of course, a real structure consists of only a finite number of cells, and in a detuned structure the cells are not identical. For a structure consisting of N cells, we should really calculate the N modes of a structure consisting of a coupled array of N unlike cells. Such a "coupled model" of the wakefields will be presented later. In general, the frequencies and kick factors of these coupled modes will differ from those of the synchronous modes in periodic structures made from each of the N cells. However, as a first approximation we may take the wakefield to be the superposition of the set of synchronous modes in the N corresponding periodic

structures:

$$W(t) = \frac{1}{N} \sum_{m=1}^{N} W_{1,m} \sin(\omega_{1,m} t) \exp\left(\frac{-\omega_{1,m} t}{2Q_{1,m}}\right) \quad . \tag{3.3}$$

This "uncoupled model" is a good approximation for sufficiently short times. It turns out that this time is longer than one might expect from a naive estimate based on the time it takes energy to propagate between cells.

Next we choose a distribution of the synchronous frequency components. Suppose we consider a structure whose iris radius a and cell radius b are to vary monotonically along the structure and whose end-cell dimensions are to be fixed. Then in general we have the freedom to shape the distribution of the dominant HEM_{11} dipole mode frequency f_1 between its two end-cell values, while keeping the frequency f_{rf} of the accelerating mode fixed (see next section).

Let the full-spread be Δf_{tot}, so that these frequencies run from $(\bar{f}_1 - \frac{\Delta f_{tot}}{2})$ to $(\bar{f}_1 + \frac{\Delta f_{tot}}{2})$. One possibility (essentially the usual "constant-gradient" structure) is a *uniform distribution*, that is, a constant spacing between adjacent components:

$$\delta f_i = f_{1,i} - f_{1,i-1} = \frac{\Delta f_{tot}}{(N-1)} \quad . \tag{3.4}$$

Another possibility is a *truncated-Gaussian distribution*, of given standard deviation σ_f, whose density of frequency components near frequency f is proportional to $\exp[-(f-f_1)^2/\,2\sigma_f^2]$. This means that the spacing between adjacent components is given implicitly by

$$\mathrm{erf}\left(\frac{f_{1,i} - \bar{f}_1}{\sqrt{2}\,\sigma_f}\right) = \mathrm{erf}\left(\frac{f_{1,i-1} - \bar{f}_1}{\sqrt{2}\,\sigma_f}\right) + A \quad , \tag{3.5}$$

where A is a constant, given by

$$A \equiv \frac{2\,\mathrm{erf}(\frac{n_\sigma}{2\sqrt{2}})}{N-1} \quad . \tag{3.6}$$

Here

$$n_\sigma \equiv \frac{\Delta f_{tot}}{\sigma_f} \tag{3.7}$$

is the full width of the truncated distribution in units of σ_f, and $\mathrm{erf}(x)$ is the usual error function:

$$\mathrm{erf}(x) \equiv \frac{2}{\sqrt{\pi}} \int_0^x e^{-u^2}\, du \quad . \tag{3.8}$$

In the core of the distribution, the fractional spacing between adjacent components is approximately

$$\frac{\delta f}{\bar{f}_1} \approx \frac{\sqrt{2\pi}}{N-1} \frac{\sigma_f}{\bar{f}_1} \mathrm{erf}\left(\frac{n_\sigma}{2\sqrt{2}}\right) \quad . \tag{3.9}$$

We focus on the truncated-Gaussian distribution because it gives a strong initial roll-off of the wake, with less partial-recoherence of the wake within the length of a bunch train than in the case of the uniform distribution.

3.2 Design of detuned structures

In this section we give a summary of our design procedure for detuned structures, by means of which the structure dimensions may be related to the uncoupled frequency distribution and certain desired rf parameters. It is also of interest to compare the rf parameters of the detuned structure with those of conventional constant-gradient and constant-impedance structures. We choose a $2\pi/3$ phase advance per cell, so the structure period is fixed at one-third of the rf wavelength.

3.2.1 Design of simplified detuned structure [38]

We begin by discussing a simplified situation in which the only dimensions that vary with cell number are the iris radius a and the cell radius b, as shown in Fig. 4(a). The corners of the disks are assumed to be square, rather than rounded as they will be in reality. The disk thickness t is assumed to be fixed, although as we shall discuss later, it will actually also be varied along the structure.

Using the computer codes TRANSVRS [39] and URMEL [40], one can show that increasing the cavity diameter $2b$ causes both the accelerating mode frequency f_{rf} and the first dipole mode frequency f_1 to decrease, while increasing the iris diameter $2a$ leads to an increased accelerating mode frequency and a decreased first dipole mode frequency. This behavior can be summarized in the three dimensional plot shown in Fig. 5. Keeping the frequency of the accelerating mode constant (here, $f_{rf} = 11.424$ GHz) yields a unique relation between a and b. Each of these a, b pairs corresponds to a different dipole mode frequency. If a certain detuning range of the dipole modes is given, clearly the two end pairs of a, b for the accelerator section can be found. It is always possible to find a unique a, b pair which lets the dipole mode frequency be any value between the frequencies of the first and last cavities and also keeps the frequency of the accelerating mode constant. The following is a summary of the design steps for this simplified case:

1. For a given operating frequency (f_{rf}=11.424 GHz) and phase shift per cell ($\phi = 2\pi/3$) of the accelerating mode, the a, b pairs can be found by using a computer code, e.g. SUPERFISH [41]. The result is shown in Fig. 6.

2. By using the code TRANSVRS, the synchronous frequency of the dipole mode f_1 for a distinct a, b pair can be calculated. The relation between a and f_1 is plotted in Fig. 7 (the corresponding cavity radii b are of course fixed from Step 1).

3. Given the desired structure length L, quality factor Q, and attenuation constant τ, the group velocities v_g of the accelerating mode for the first and last cavities are calculated according to the constant gradient approximation

$$v_g(s) = \frac{\omega_{rf}}{Q}\left[\frac{L}{1-e^{-2\tau}} - s\right] \quad . \tag{3.10}$$

   These velocities uniquely determine the a, b pairs at the ends of the structure, and thereby the overall dipole mode frequency spread Δf_{tot} and the mean dipole frequency $\bar{f}_1$.

4. Using Eqs. (3.5)–(3.7) for a truncated Gaussian distribution, with a chosen N and σ_f, the frequency of the dipole mode for each cavity in the structure can be calculated.

3.2.2 Evaluation of rf parameters [38]

For a given set of structure dimensions, the rf parameters can be calculated using SUPERFISH. Although this code only calculates rf parameters for uniform structures with constant a, b, p and t, the calculations are valid locally for our detuned structure with slowly changing a and b. The calculated quality factor Q of the accelerating mode, as a function of longitudinal coordinate s along the structure, is shown in Fig. 8. In Fig. 9 we show the calculated group velocity v_g/c along the structure, for the accelerating mode.

The power flow in the accelerator section can be expressed as

$$P(s) = P_{in} e^{-2\tau(s)} \quad , \tag{3.11}$$

where P_{in} is the input power, and $\tau(s)$ is the attenuation along the section, given by

$$\tau(s) = \omega_{rf} \int_0^s \frac{ds'}{2Q(s')v_g(s')} \quad . \tag{3.12}$$

The shunt impedance $r(s)$ calculated using SUPERFISH is shown in Fig. 10. Then the accelerating electric field $E_z(s)$ can be calculated:

$$E_z(s) = \sqrt{r(s)\frac{dP(s)}{ds}} \quad , \tag{3.13}$$

where $r(s)$ is the shunt impedance per unit length. In Fig. 11, $E_z(s)$ is shown for an input power of 100 MW. For comparison, $E_z(s)$ for a conventional constant-gradient section and for a constant-impedance section, with the same input power and attenuation as the detuned structure, are also plotted in Fig. 11. Finally, by

integrating the electric field $E_z(s)$, we can calculate the energy gain $U(s)$ along the detuned structure, which is shown in Fig. 12. The behaviors of the detuned and the constant-gradient structure are similar; the detuned structure may be regarded as a "quasi-constant-gradient" structure. We note from Fig. 11 that the detuned structure has a slightly higher energy gain than the conventional constant-gradient structure.

The dispersion curves for accelerating and dipole modes are displayed in Fig. 13 and Fig. 14 respectively. For the accelerating mode, all curves cross at the frequency f_{rf}=11.424 GHz with a phase advance of $\phi = 2\pi/3$. The slopes of these curves are the group velocities, which were already shown in Fig. 9 at the accelerating mode frequency. The dispersion curves for the dipole modes are very shallow, with positive group velocities in the front end of the section and negative ones at the back end (see Fig. 15).

3.2.3 Design of first NLC test structure

Next we discuss the design of the actual 1.8-m NLC-type structure that is being built for testing purposes at SLAC. In this structure, the disk thicknesses are varied along the structure, and the edge of the iris in each disk is rounded into a full semi-circle. The relevant cell dimensions are shown in Fig. 4(b). We have already shown how one can take care of the lowest frequency, most dangerous dipole mode in our discussion of the simplified detuned structure. However, the effect of the higher dipole modes, while smaller, is nonnegligible. We have found that varying the disk thickness t is an effective method of detuning the remaining significant modes (Ref. 24); specifically, this method can be used to detune modes of the form HEM_{nm1}. For the first test structure design, we have settled upon a variation of t going from 1 to 2 mm from the first to the last cell, in a truncated Gaussian pattern with $\sigma_t = 0.25$ mm. Preliminary results indicate that this will sufficiently detune not only the higher dipole HOMs, but also the longitudinal HOMs. The variation of t has little effect on f_{rf} and f_1.

The basic design procedure for the actual structure is then as follows:

1. Using the computer code YAP [42], the relationship among a, b, and t, given the fixed accelerating frequency and phase advance per cell, may be found for the structure, taking into account the effect of the rounded corners.

2. Again using YAP, the relationship among the synchronous dipole mode frequency f_1, a, b, and t may be found (where b is fixed by Step 1).

3. The desired relative spacings of the dipole mode frequencies, $\{f_{1,i} - f_{1,i-1}\}$, and the distribution of disk thicknesses, $\{t_i\}$, are specified. As already noted, both of these are chosen to be truncated Gaussian distributions.

4. Given a value a_1 for the iris radius of the first cell, the central frequency $\bar{f}_1$ and all of the a_is and b_is are uniquely determined by the above constraints. We adjust a_1 to obtain the desired filling time T_f.

The resulting structure parameters are summarized in Table 2. When a parameter varies along the structure, the range of values from the first to the last cell is given. Figure 16 shows $E_z(s)$ for the actual detuned structure. We also show $E_z(s)$ for conventional constant-gradient and constant-impedance sections, with the same input power and attenuation as the detuned structure. We note that the field at the end of the structure is higher relative to its value at the input than it is in the simplified structure of the preceding section, because of the additional slowing of group velocity due to the thickening of the irises along the structure.

The envelope of the wake function for the lowest passband, using parameters from Table 2 and obtained using the uncoupled model, is shown in Fig. 17. There is an initial sharp roll-off due to the Gaussian distribution of frequencies. The range of $z = ct$ shown, from 0 to 40 meters, is a little more than the length of a 90-bunch train. The envelope is calculated according to

$$\hat{W}(z) = \sqrt{S_N^2 + C_N^2} \quad , \tag{3.14}$$

Table 2: Parameters for an NLC structure	
Accelerating frequency	11.424 GHz
Phase advance per cell	$2\pi/3$
Structure length	1.8 m
Number of cells	204 + 2 couplers
Iris radius, a	0.572 to 0.39 cm
Cell radius, b	1.144 to 1.068 cm
Iris thickness, t	1 to 2 mm
Frequency of lowest dipole mode, f_1	14.312 to 15.834 GHz
Mean dipole mode frequency, $\bar{f}_1$	15.073 GHz
$\frac{\sigma_f}{\bar{f}_1}$	2.5%
Total fractional spread, $\frac{\Delta f_{tot}}{\bar{f}_1}$	10.1%
Group velocity, v_g/c	0.12 to 0.03
Filling time, T_f	100 nsec
Attenuation parameter, τ	0.517
Elastance, $s \equiv \omega \frac{r}{Q}$	653 to 946 V/pC/m
Q of lowest dipole mode	≈ 6500

where

$$C_N \equiv \sum_{m=1}^{N} W_{1,m} e^{-k_{1,m} z/2Q_{1,m}} \cos(\delta k_m z) \tag{3.15}$$

and

$$S_N \equiv \sum_{m=1}^{N} W_{1,m} e^{-k_{1,m} z/2Q_{1,m}} \sin(\delta k_m z) \quad . \tag{3.16}$$

Here $k_{1,m} = \omega_{1,m}/c$, and $\delta k_m \equiv k_{1,m} - \bar{k}_1$. One can show that

$$\begin{aligned} W(z) &= C_N \sin(\bar{k}_1 z) + S_N \cos(\bar{k}_1 z) \\ &= \hat{W}(z) \sin(\bar{k}_1 z + \phi) \quad , \end{aligned} \tag{3.17}$$

where $\tan\phi = S_N/C_N$.

We shall see that this uncoupled model represents the general character of the wake quite well, and is quantitatively very good for the shorter range (first several meters) of the wake. However, to more accurately represent the longer range wake, we must include the effects of coupling.

3.3 Coupled model for cell-to-cell detuning

In this section, we describe an approach (Ref. 37) to calculating the coupled modes of the structure, starting from a distribution of uncoupled synchronous frequencies obtained as discussed in the preceding sections. We present equivalent circuit models which are reasonable representations of the tapered iris-loaded accelerating structure. Our model builds upon previous work that represents accelerating structures by equivalent circuit models [43,44]; a new feature of our approach is a more correct treatment of the situation in which the coupling changes sign in the structure. In order to derive these models, we imagine that each cell is excited in some combination of cell modes and that the coupling holes determine the relation between the coefficients of these modes in two adjacent cells. Since the longitudinal electric field vanishes on the axis, we expect the coupling to be magnetic in character.

Here we shall concentrate on the simplified structure shown in Fig. 4(a). The method has, however, been extended to the case of varying disk thicknesses t (Ref. 24).

3.3.1 Single-band equivalent-circuit model

Let us start with a single circuit chain in which each circuit corresponds to a single cell mode and the circuits are coupled magnetically. The equations for the amplitude a_m of excitation in cell m, which is coupled to cells $(m-1)$ and $(m+1)$, is

$$(x_m - \lambda)\, a_m + \frac{\kappa_{m+\frac{1}{2}}}{2} a_{m+1} + \frac{\kappa_{m-\frac{1}{2}}}{2} a_{m-1} = 0 \quad . \tag{3.18}$$

Here $x_m = f_m^{-2}$ where f_m is the resonant frequency of cell m, $\lambda = f^{-2}$ where f is the coupled-mode frequency, and $\kappa_{m\pm\frac{1}{2}}$ represents the equivalent coupling coefficient between cell m and cell $(m \pm 1)$. If the structure is periodic with N cells $(m = 1, 2, \ldots, N)$ and $f_m = \tilde{f}$, we find the solution

$$a_m = a \cos m\phi_\ell \quad , \tag{3.19}$$

with $\phi_\ell = \ell\pi/N$, and $\ell = 0, 1, 2 \ldots N$. The corresponding eigenfrequencies satisfy the equation

$$\frac{1}{f^2} = \frac{1}{\tilde{f}^2} + \kappa \cos\phi \quad . \tag{3.20}$$

If we choose the boundary conditions

$$a_0 = a_1 \ , \quad a_{N+1} = a_N \ , \quad \kappa_{\frac{1}{2}} = \kappa_1 \ , \quad \kappa_{N+\frac{1}{2}} = \kappa_N \quad , \tag{3.21}$$

(where κ_1 is the coupling coefficient between cells in a periodic structure made of cell type 1, and similarly for κ_N), then we find our solutions are limited to phase advance

$$\phi_\ell = \frac{(\ell - 1)\pi}{N} \quad , \quad \ell = 1, 2 \ldots N \quad . \tag{3.22}$$

Since we do not have a reliable procedure to calculate $\tilde{f}$ and κ directly from the geometry, we reconstruct $\tilde{f}$ and κ from values of the zero-mode and π-mode in an infinite periodic structure, as obtained from TRANSVRS. We now repeat this

procedure for periodic structures corresponding to the geometry of cells at various places in the tapered structure. We then obtain via interpolation the values of f_m and $\kappa_{m\pm\frac{1}{2}}$ needed for Eq. (3.18). By treating Eq. (3.18) and its appropriate boundary conditions as an $N \times N$ matrix equation, we obtain the frequency (f_ℓ) and mode pattern $(a_m^{(\ell)})$ for each mode ℓ. From the $a_m^{(\ell)}$ we obtain the kick factors K_ℓ.

The results using parameters for the 206-cell NLC structure (see Table 2) are shown in Figs. 18 and 19. Figure 18 displays the mode spectrum, the kick factor, the mode density dn/df, and the product of kick factor times mode density. Note that dn/df is normalized so that its integral over frequency is one; thus, $dn/df \approx \frac{1}{(N-1)\delta f_i}$, where δf_i is the spacing between adjacent modes near mode i. The results of the uncoupled model are shown also, as dashed lines in this figure. The resulting wake function is shown in Fig. 19.

An important feature of the NLC structure is that the values of the coupling coefficients κ_m change from positive (forward wave) to negative (backward wave) as one moves from the beginning to the end of the structure. As a result, the mode pattern is localized to the interior of the structure for most of the modes (see Ref. 37). It is only these localized modes that significantly interact with the beam. Those modes that do extend to an end of the structure (the lowest and highest frequency modes) have greatly depressed kick factors. A consequence of this is that the boundary conditions have little effect on the wakefield.

As we shall see later, the wake function at the locations of the bunches needs to be kept to about 1% or less of its peak value, i.e., less than about 1 V/pC/mm/m. From Fig. 19, we see that the wakefield envelope $\hat{W}(z)$ for bunches 1–25 (assuming the NLC bunch spacing of 42 cm) satisfies this criterion. This was also true for the uncoupled model (see Fig. 17). The two models agree well in this range because the cell-to-cell coupling is weak. Other authors have reached similar conclusions via direct time-domain integration of the coupled-circuit equations [45]. Over the longer range, the wake function grows unacceptably. However, it is possible to

counter this growth by using several interleaved structure types, as will be discussed later.

3.3.2 Double-band equivalent-circuit model

We seek to obtain a better fit to the dispersion curves for the lower two bands. To do this we have derived a two-band circuit model corresponding to the excitation of both TM_{110} and TE_{111} modes in each cell (Ref. 37). As a result, we obtain the coupled difference equations

$$(x_m-\lambda)a_m-\frac{\kappa_{m+\frac{1}{2}}}{2}a_{m+1}-\frac{\kappa_{m-\frac{1}{2}}}{2}a_{m-1}=-\frac{\sqrt{\kappa_{m+\frac{1}{2}}\hat{\kappa}_{m+\frac{1}{2}}}}{2}\hat{a}_{m+1}+\frac{\sqrt{\kappa_{m-\frac{1}{2}}\hat{\kappa}_{m-\frac{1}{2}}}}{2}\hat{a}_{m-1} \tag{3.23}$$

$$(\hat{x}_m-\lambda)\hat{a}_m+\frac{\hat{\kappa}_{m+\frac{1}{2}}}{2}\hat{a}_{m+1}+\frac{\hat{\kappa}_{m-\frac{1}{2}}}{2}\hat{a}_{m-1}=\frac{\sqrt{\kappa_{m+\frac{1}{2}}\hat{\kappa}_{m+\frac{1}{2}}}}{2}a_{m+1}-\frac{\sqrt{\kappa_{m-\frac{1}{2}}\hat{\kappa}_{m-\frac{1}{2}}}}{2}a_{m-1}\,. \tag{3.24}$$

We now have a 2N-dimensional eigenvalue problem, with eigenvalues $\lambda = 1/f^{-2}$ and eigenfunctions $(\mathbf{a}, \hat{\mathbf{a}})$. Note that a_m and $\hat{a}_m$ represent the amplitudes of the components of the TM_{110} and TE_{111} modes, respectively. The parameters x, $\hat{x}$, κ and $\hat{\kappa}$ are obtained as discussed below.

The dispersion curves for the lower two bands are readily obtained from the above difference equations for a periodic structure, and correspond to the equation

$$\cos\phi = \frac{\kappa\hat{\kappa}-(x-\lambda)(\hat{x}-\lambda)}{(x-\lambda)\hat{\kappa}-(\hat{x}-\lambda)\kappa} \quad . \tag{3.25}$$

This equation represent a hyperbola when λ is plotted against $\cos\phi$. The four unspecified parameters, x, $\hat{x}$, κ and $\hat{\kappa}$ are chosen to match the ends of the lower two dispersion bands calculated from TRANSVRS, for geometries at different locations in the structure, and the predicted and calculated curves shown in Fig. 20 are in excellent agreement. We note that the parameters κ and $\hat{\kappa}$ do not change sign when we go from the beginning to the end of a structure. In this case the change from

forward-wave to backward-wave that was seen in the single band model corresponds to the relative sizes of the TM_{110} and TE_{111} components along the structure, since the signs of κ and $\hat{\kappa}$ on the left sides of Eqs. (3.23) and (3.24) are opposite for the TM_{110} and TE_{111} modes.

The above difference equations, supplemented by the appropriate boundary conditions in the first and last cells, are solved by matrix inversion, and the kick factor and wakefield are calculated as before. In the expression for the kick factor (see Ref. 37), only the TM_{110} (a_m) coefficients enter into the numerator, although both a_m and $\hat{a}_m$ enter into the stored energy in the denominator. Once again most of the modes are localized in the structure in the lowest band (Ref. 37). The results are shown in Figs. 21 and 22 for the double-band model. Note that the modes of the second band (roughly, those above 17 GHz) have low kick factors and therefore do not contribute significantly to the wakefield. There is some difference between the results of the one- and two-band models, showing up mainly in the longer range behavior of the wake. The double-band model, which is expected to give a more accurate representation of the longer-range wake field, in fact shows somewhat more suppression of the longer-range wake, as can be seen by comparing Figs. 19 and 22.

3.4 Supplementing detuning with structure-to-structure variation

Suppose we are using a truncated Gaussian distribution of frequencies, as given by Eq. (3.5), for the fundamental dipole mode. If there is just one type of X-band structure of length about 1.8 m, then in Eq. (3.5), $N \approx 200$.

The initial value of the average betatron function β in the NLC main linac design is about 4 m, and it increases as the square root of the energy as one goes down the linac. Thus, the betatron wavelength $2\pi\beta$ is much greater than the structure length everywhere in the linac, even near the beginning. Suppose now that instead of just one structure type we build n different structure types; we thus increase the total number of frequencies N by a factor n, to obtain the

overall distribution of frequencies. One might then "interleave" the frequencies from the overall distribution in the different structure types; e.g., if $n = 3$, the lowest frequency would be in structure type 1, the next lowest in type 2, the next lowest in type 3, the next lowest in type 1, and so on, cycling repeatedly through the structure types. Suppose also that the linac is built by repeatedly cycling through the n structure types along its length.

Dynamically, we expect the effect to be much the same as if the wake function were a sum of n times the number of modes in a single structure. This expectation is borne out by our simulations, in which we cycle through a set of structure types with interleaved frequencies as discussed above. The greater density of lines in the distribution leads to greater suppression of the effective wake at longer distances. Provided that n is not too large, one expects the dynamics to be almost the same as if the wake function $W(t)$ were an average of the wake function over the n structures. [If n times the structure length is comparable to or greater than half a betatron wavelength, this averaging is no longer valid. Also, the ordering of the structure types within one cycle begins to matter more.]

3.5 Effect of errors

So far, we have neglected the effects of small random variations in the frequencies, due, for example, to fabrication errors. There are two extreme cases, namely, the case in which the error in each frequency in the design distribution is the same in all sections (we denote this "systematic"), and the case in which the error in each frequency is totally random from section to section. Note that our definition of "systematic" means that the errors are the same in corresponding cells of a given structure type, but they are still random from cell to cell in each structure type. Systematic errors can lead to considerable worsening of the long-range wakefield behavior. The totally random errors are generally less harmful, and in fact can actually lead to some additional suppression of the long range wakefield behavior, since the effective wake function is then a sum of an even denser distribution of frequencies.

Another type of error is transverse misalignments of the cells in a structure. As we shall see later, the effect on the blow-up of the beam depends somewhat on the correlation length of the misalignments, but the tolerance is fairly tight on all scales.

3.6 Mechanical design of detuned structure

A sketch of the actual accelerator section being built at SLAC for use in the NLC Test Accelerator facility [46,47] is shown in Fig. 23. A schematic of the individual cells of the structure is shown in Fig. 24. Each cell of a section will have different cavity diameter, iris diameter, and iris wall thickness, calculated as discussed in preceding sections to give the required dispersion characteristics for the fundamental mode and for the higher-order dipole modes.

Six cells (one close to each end, and four evenly distributed between them) will have radial pumping holes connecting the central (beam) cavity to two outer vacuum manifolds. These manifolds will each be connected to two 8-liter/s vacuum pumps in the middle of the section. The manifolds will increase the pumping speed through the small beam apertures by an order of magnitude. This improvement may be necessary to handle the increased gas load resulting from high peak power rf propagating through the structure.

Four water-cooling tubes will be brazed along the outside of each section, as shown in Fig. 23. The outer surface of each cell can be used for precise support and alignment since it is concentric to the iris diameter to within 5–10 μm. Two tuning stubs will be brazed into each cell wall to permit fine tuning of the phase advance per cell of a completed section. Symmetrical double-input couplers will be used at the ends of each section to minimize the phase and amplitude asymmetries in the coupler fields.

Each accelerator section will be mounted on an aluminum strongback. Supports from the strongback to the section will be positioned under the pumping cells, as shown in Fig. 23. The support at the input-coupler end will be rigidly

attached to the strongback. All other supports will be flexible to allow for longitudinal differential expansion. Each support will permit vertical fine adjustment so that the section can be held straight to within 5 μm.

4. Beam dynamics simulations

Since our ultimate goal is to control the projected emittance of a multibunch beam, we turn now to the dynamics of such a beam as it passes through the wakefield-suppressed structures. Each bunch is represented as a single macroparticle (i.e., internal bunch structure is ignored). The equation of motion for the transverse offset x_n of the nth bunch in a train is

$$\gamma(s)x_n'' + \gamma'(s)x_n' + \gamma(s)\mathcal{K}^2(s)x_n = F_n(s) \quad , \tag{4.1}$$

where the driving term due to the wakefields of the preceding bunches is

$$F_n(s) \equiv \frac{N_p e^2}{mc^2} \sum_{j=1}^{n-1} W((n-j)\ell/c)\, x_j(s) \quad . \tag{4.2}$$

Here N_p is the number of particles per bunch, E the energy of the particles in a bunch, ℓ the spacing between adjacent bunches, m the rest mass of the electron, and γ the usual Lorentz factor E/mc^2. Primes denote derivatives with respect to longitudinal position s. The acceleration is assumed to be linear: $\gamma = \gamma_0 + Gs$, with G a constant. The sum over modes in Eq. (4.2) may be a sum over uncoupled or coupled modes, as calculated in the preceding sections.

The focusing function $\mathcal{K}(s)$ in the NLC is to vary approximately as the inverse square root of the energy, and unless otherwise noted we have simply used the smooth approximation

$$\mathcal{K}(s) = \left(\frac{\gamma_0}{\gamma(s)}\right)^{1/2} \mathcal{K}_0 \quad . \tag{4.3}$$

We have used the programs LTRACK [48] and MBLINAC [49] for our simulations. In these codes, the focusing elements and the accelerating structures (or

pieces thereof) are modelled by discrete kicks. Both codes allow one to simulate situations in which the wakefield varies from structure to structure, as occurs when using interleaved structures or in the presence of random frequency errors.

4.1 Moments of the wakefield kicks

One way to obtain some insight into the effect of the wakefield on the bunch trajectories within a structure is via the "moments" of the wakefield kicks. This approach readily follows from a treatment of the multi-bunch problem for linac FODO arrays where the bunch trajectories are essentially straight lines through the structures. Such trajectories simplify the integration of the wakefield kicks along the structure. Assuming exact linear trajectories for the purpose of computing the driving terms in the equations of motion is generally a good approximation since the trajectory deviations due to intra-bunch transverse wakefields, acceleration, and beam loading are usually small relative to the unperturbed betatron motion.

To formulate this approach, we first consider the simple case of only two bunches traversing a single unpowered structure of half-length L_h. In the approximation in which the first bunch follows a straight line trajectory, its net effect on the trajectory of the second bunch can be written

$$\begin{pmatrix} \Delta x \\ \Delta\theta \end{pmatrix} = \frac{2L_h N_p e^2}{E} \begin{pmatrix} -M_1 L_h & -M_2 {L_h}^2 \\ M_0 & M_1 L_h \end{pmatrix} \begin{pmatrix} x \\ \theta \end{pmatrix}, \tag{4.4}$$

where Δx and $\Delta\theta$ are respectively the effective change in the transverse position and angle of the second bunch at the center of the structure, and x and θ are the position and angle of the first bunch at this same location. The position and angle are of course relative to the axis of the structure. The M_is are the moments of the

wakefield kicks and are defined in the uncoupled model as

$$
\begin{aligned}
M_0 &= \frac{1}{N}\sum_{m=1}^{N} W_1 \sin(\omega_{1,m}\ell/c), \\
M_1 &= \frac{1}{N}\sum_{m=1}^{N} \left(\frac{s_m}{L_h}\right) W_1 \sin(\omega_{1,m}\ell/c), \\
M_2 &= \frac{1}{N}\sum_{m=1}^{N} \left(\frac{s_m}{L_h}\right)^2 W_1 \sin(\omega_{1,m}\ell/c) \quad ,
\end{aligned}
\tag{4.5}
$$

where s_m is the longitudinal position of cell m relative to the center of the structure, and ℓ is the bunch separation. For simplicity, we ignore the effect of the Qs of the modes and assume that the wakefield strength W_1 is the same for all cells. With these assumptions, M_0 equals $W(t = \ell/c)$ in Eq. (3.3), which is the function one tries to minimize by detuning the cells. The additional moments, M_1 and M_2, result from the distribution of the wakefield kicks over a finite length. This distribution can change the trajectory of the second bunch even if the first bunch has an average offset of zero through the structure.

Having specified the bunch-to-bunch coupling, the next step is to compute its effect on betatron motion. For the two-bunch example, we are interested in the size of the betatron amplitude induced in the second bunch from its coupling to betatron motion of the first bunch. For the simple linac configuration of a constant-energy FODO array with a single structure between each quadrupole, the calculation yields an expression for the induced amplitude that is independent of M_1 if the bunches travel an integral number of FODO cells in which the net betatron phase advance is an integral multiple of π. The cancellation of the contribution from M_1 is related to the symmetry of the FODO cells and also occurs to a large degree if the bunches are accelerated. Thus for linacs with many FODO cells, this moment of the wakefield kicks can generally be ignored. In contrast, the M_2 contribution from groups of cells having π phase advance is additive in a constant-energy linac, and so it increases linearly with distance as does the contribution from M_0.

As a specific example of induced motion, we consider the case of a linac in which the bunch energy increases linearly with distance, and the beta function and spacing between quadrupoles increase as the square root of the bunch energy. We also assume that the same type of structure is used throughout the linac and that the structures fill the entire space between quadrupoles. This requires the approximation of fractional structures since the quadrupole spacing is generally not an integral number of structure lengths. For this configuration, the induced amplitude A of the second bunch at the end of the linac per unit amplitude of the first bunch is to a good approximation,

$$A = \frac{N_q \beta_0 N_p e^2}{E_0} M_0 L_h \left[1 + \frac{g}{3} + g\left(\frac{M_2}{M_0} - \frac{1}{3}\right)\sqrt{\frac{E_0}{E_f}}\ \right] \quad , \tag{4.6}$$

where

$$g \equiv \frac{\sin^2(\phi/2)}{1+\cos^2(\phi/2)} \quad . \tag{4.7}$$

Here ϕ is the phase advance per FODO cell. The number of quadrupoles N_q is given by

$$N_q = \frac{E_0(\sqrt{E_f/E_0} - 1)}{E_z L_h} \quad , \tag{4.8}$$

where $2L_h$ = structure length = initial quadrupole spacing. Also, β_0 is the initial beta function at the midpoint between quadrupoles, E_0 is the initial linac energy, E_z is the accelerating gradient, and E_f is the final linac energy.

The expression for A shows that with the increase in energy, the relative contribution M_2 scales as $\sqrt{E_0/E_f}$. This is due to the increase of the betatron wavelength relative to the structure length as the energy increases. The relative sizes of M_2 and M_0 depend on the detuning parameters and the bunch separation. For the parameter ranges being considered for the NLC, the M_2/M_0 amplitude ratio, ignoring the wakefield phase, is generally near unity for distances of many bunch spacings, but can be as large as 20 at the first bunch location. This increase at short distance occurs since M_2 decoheres slower with ℓ than does M_0. Thus it is important to also consider the size of M_2 when choosing the detuning parameters.

5. Control of beam break-up

We discuss in this section the required level of suppression of the transverse wakefield in the NLC, and we examine how well the various schemes of wakefield suppression can be expected to meet these criteria.

5.1 Use of damping alone

Using damping alone, we are generally in a regime in which, if we have lowered the Q to the point at which the wake at one bunch spacing produces acceptably small blow-up in the "short pulse" design, then the blow-up of bunches in longer bunch trains will also be acceptably small. In this case, the exponentially-damped wake is essentially negligible beyond one or a very few bunch spacings. This "daisy-chain" regime has been discussed extensively elsewhere (see Refs. 19 and 50). The required Qs are about 10.

The use of damping seems very natural for long bunch trains, since, if one can obtain such low Qs, the wake quickly becomes negligible beyond a short distance. However, for the reasons discussed previously, assuring that all the harmful modes are coupled out of the structure and absorbed may not be easy.

5.2 Suppression of wake via detuning

Let us consider the coupled wakefield (without errors) shown in Fig. 22. In Fig. 25(a), we show the value of the wake function $W(z)$ at multiples of the spacing between bunches. What actually matters is the sum of all the wakefield kicks from the bunches preceding a given bunch; this sum depends on both the wake function at each bunch spacing and on the betatron phases of the bunches. Figure 25(b) shows the sum of the wake functions at each bunch n, i.e.,

$$\sum_{j=1}^{n-1} W(j \cdot \ell) \quad . \tag{5.1}$$

If we assume that the bunches start out at the same betatron phase, this sum correlates strongly with the blow-up of the betatron oscillation of each bunch. In

Fig. 25(c), the blow-up factor x/x_0 is shown for each of the bunches, as calculated using the linac parameters given in Table 1 and a structure which has the averaged wakefield shown in Fig. 22.

Here we have assumed that all the bunches in the train start out with the same offset at the beginning of the linac. The blow-up factor x/x_0 is the ratio of the the maximum amplitude reached anywhere in the linac to the initial amplitude, with adiabatic damping factored out.

The kick factor of the fundamental transverse HOM is about 40 V/pC/mm/m for the NLC structures. Thus the amplitude of the envelope of the wake function $W(z)$ at its maximum, occurring for small z, is about 80 V/pC/mm/m, as can be seen in Fig. 22. We see from Fig. 25 that once the wake exceeds about 1% of this peak value, there starts to be significant blow-up of bunches that are far enough back in the train to see wakes from bunches this distance ahead. Thus, if the envelope of the wake is kept below 1% of this peak value, at the locations of the bunches, the wakefield suppression will generally be adequate. This assumes that the actual values of the wake at the various bunch spacings will be less than the envelope values, since the bunch spacings will fall at varying phases of the wake function. Assuming such a varying distribution of phases, an approximate rule of thumb for our linac parameters is that the wake function envelope needs to be suppressed by a factor of about 100 below its short range maximum, throughout an interval equal to the desired length of the bunch train.

With a 10% frequency spread of the detuned wakefield modes and a 1.4 ns bunch spacing, there is at least one resonance between the bunch frequency and the wakefield mode frequencies. At such a resonance, the bunches are exactly at the zero-crossings of the wakefield, but slightly off this resonance, the wakes from successive bunches add up with the same sign (assuming the bunches are at essentially the same betatron phase) and can produce a strong effect. If the modes are densely spaced over the region of the resonance, then the integrated effect of the resonant wake distribution will be essentially zero. However, for a large number of

bunches, which leads to a narrow resonance, this integral may not be so small, and hence there can be fairly strong residual kicks from the resonant growth. Errors in the frequencies will exacerbate this problem, and so care must be taken to avoid this type of growth. [51]

Using single-section detuning alone, one may obtain an acceptably small wake-field during the interval needed for a short pulse design, but unfortunately it will not remain small enough over longer bunch trains. In fact, there will generally be significant recoherence of the wake at a time comparable to the reciprocal of the core frequency spacing [see Eq. (3.9)]. Furthermore, errors in the frequency distribution can lead to even larger values of the wake function within the bunch train. We see that single-section detuning, even without including the effects of errors, still leads to considerable transverse blow-up in the longer bunch trains.

5.3 Multiple detuned structure types with interleaved frequency distributions

One possible solution to the problem of controlling the wake at longer distances is to use several structure types with interleaved frequency distributions, as discussed earlier. This solution works, provided the effects of systematic errors in the frequency distribution can be kept small enough. About four interleaved structure types are needed; similar conclusions have been reached by other groups. [52] In Fig. 26, we show the envelope of the wake function averaged over four interleaved structure types, calculated using the double-band, coupled model for each structure type. The overall uncoupled frequency distribution is a truncated Gaussian with $\sigma_f = 2.5\%$ and a total spread of $4\sigma_f$. No errors in the frequency distribution have been included here. In Fig. 27(a), we show the value of the wake function $W(z)$, averaged over the four structure types, at multiples of the spacing between bunches. In Fig. 27(b), we show the sum of these averaged wake functions from preceding bunches at each bunch n. In Fig. 27(c), the blow-up factor x/x_0 is shown. In the simulation of the beam blow-up, we cycle repeatedly through the four structure types in going down the linac.

5.4 Frequency errors

The results in the preceding section suggest that cycling through four structures types having interleaved frequency distributions can suppress the wakefield long enough to make it feasible to use bunch trains of length a filling time or so. However, we have not yet taken into account the fact that there will be unavoidable systematic and/or random deviations from the calculated frequency distributions.

The core spacing, i.e., the spacing of the frequencies in the center of the Gaussian, is given by Eq. (3.9) for the uncoupled model. (This spacing is increased somewhat according to the coupled models, in particular by a factor of about 1.4 in the double-band model—see Figs. 18(c) and 21(c).) For our single section type, the fractional core spacing $\delta f/\bar{f}_1$ given by Eq. (3.9) is 3×10^{-4}, while for the case of four interleaved section types, it is four times smaller, 7.5×10^{-5}.

The expected size of the errors due to machining tolerances is comparable to these values. The problem is rather complex, since the errors are neither "totally random" nor purely "systematic" in the senses defined earlier. In reality the errors are not a simple superposition of these "systematic" and "totally random" errors, but for a first estimate, we shall treat them as such. We remind the reader that our definition of "systematic" means that the errors are the same in corresponding cells in all instances of a given structure type; they are still random from cell to cell within each structure type. Purely systematic errors of this sort would be a pessimistic extreme case. However, there will generally be some average error over all the cells of a given type, and this may be roughly approximated by the systematic component as defined here. Superimposed on this systematic distribution is the "totally random" component of the errors.

As one might expect, the result for the beam blow-up remains quite similar to that shown in Fig. 27(c), provided that the fractional errors in the frequency distribution are kept small compared to the core spacing, that is, not more than about 10^{-5} or so. However, from the size of the fabrication tolerances we expect random errors with fractional rms about 1×10^{-4} or so. With care taken to

randomize the production of various cell types, it should be possible to keep the systematic components of the errors significantly smaller than this, perhaps by nearly an order of magnitude.

As a simple model, we shall assume that each of the two types of errors is randomly distributed, each with given rms. Denote the fractional rms of the systematic errors by $\sigma_{e,sys}$ and the fractional rms of the random errors by $\sigma_{e,ran}$. These distributions are Gaussian, but assumed to be truncated at three sigmas. When the coupled modes are calculated using the double-band equivalent circuit model, it is found that the size of the rms of the coupled-mode errors is about a factor of two smaller than the rms of the errors in the uncoupled modes which are input to the calculation. Both the $\sigma_{e,sys}$ and the $\sigma_{e,ran}$ that we quote correspond to those of the random errors in the uncoupled modes input to the equivalent circuit calculation.

We give examples showing the effect of frequency errors on the blow-up due to an injection offset, assuming $\sigma_{e,ran} = 1 \times 10^{-4}$ and $\sigma_{e,sys} = 3 \times 10^{-5}$. The result is of course somewhat dependent on the particular seeds used to generate the random and systematic errors. In Fig. 28, we show a typical result for a single section type with errors of this magnitude — there is considerable blow-up of the bunches in the last two-thirds of the train. In Fig. 29, we show the result for four section types with interleaved frequency distributions and the same values of $\sigma_{e,ran}$ and $\sigma_{e,sys}$. The worst result out of 16 pairs of seeds for the random and systematic errors is shown. The blow-up of x/x_0 is kept below 22% for all bunches. Even for an initial transverse offset equal to the rms beam size, the bunch train's projected-emittance blow-up at the end of the linac is only a few percent.

5.5 Misalignments

One of the most severe tolerances is that on misalignments of the accelerating structures. We consider not only misaligments of a structure as a whole, but also misalignments of pieces of the structure with respect to each other due to manufacturing errors. As a simple model, we assume that each misaligned piece of structure contains i_m cells, (where i_m may vary from 1 to the number of cells in a whole structure), the misalignment within each such piece is uniform, and the misalignments are random with rms size σ_m. Figure 30 shows the tolerance $t_{25\%}$ on σ_m to produce a 25% emittance blow-up as a function of i_m, assuming four interleaved structure types. Here we have assumed a FODO-type lattice, with beam size in the initial focusing quad equal to 3.6 μm (comparable results are obtained using smooth focusing).

From Fig. 30, we see that the tolerance is fairly insensitive to i_m, although it is tightest when i_m is around 20. The loosest tolerance is for misalignment of entire structures, since the coherence of the detuned frequency distribution within a section is preserved.

More detailed studies of tolerances are in progress. It appears likely that the blow-up in long bunch trains can be controlled via detuning alone, provided that several structure types with interleaved frequency distributions are used. The most difficult tolerance appears to be the misalignment tolerance of a few microns for assembly of pieces of structures during the manufacturing process. However this tolerance can probably be loosened by using appropriate trajectory correction algorithms, and this avenue is also being pursued.

5.6 Combining detuning and damping

Strictly speaking, one never uses detuning alone — there will always be at least a minor amount of damping due to the resistivity of the structure. For our long bunch trains, even this small amount of damping ($Q \approx 6500$) has a non-negligible effect on the result (and was included in the above examples). However,

one may consider deliberately introducing both damping and detuning. Instead of using interleaved structures, one could introduce sufficient damping to control the partial recoherence of the wake at long distances (Ref. 9). However, it is probably necessary to damp many of the cells in the structures, and this may not be that much easier than damping all the cells so strongly that detuning would not really be necessary (although the near-constant gradient of the detuned structure is desirable for other reasons). However, detuning is very good for producing an initial strong roll-off of the wake between adjacent bunches, while moderate damping is a natural way to avoid a resurgence of the very long range wake, so the two methods are complementary. The disadvantage of using both is the additional complication in fabricating the structures.

It is also possible that appropriate design of the vacuum manifold could produce some degree of damping; this possibility is presently under investigation.

6. Summary and conclusions

We have concentrated our efforts on two methods of suppressing the transverse dipole wakefield, which would otherwise produce severe multibunch beam break-up in future linear colliders. Our theoretical and simulation work so far indicates that either of the two methods, damping or detuning, may be capable of suppressing the wakefields to the required degree. The choice of method will depend to some extent on practical considerations. A practical and inexpensive means of absorbing the power channelled out of the radial waveguides is needed, if damping is to be used as the major means of wakefield suppression. Keeping the misalignments and the deviations from the desired frequency distribution sufficiently small is important if detuning alone is to be used. At this time, we are pursuing the detuning option most intensively, as it appears to be possible to achieve the required suppression by using four interleaved structure types.

Much more work remains to be done and is currently in progress. Improved methods for modelling damped and detuned structures (for example, a scattering-

theory formalism for calculating the wakes in detuned structures [53]) are being developed at SLAC and elsewhere. Measurements of the wakefields in single test structures will be an important focus in the near future. If the detuning option is chosen, it will be necessary to demonstrate the feasibility of building structures to sufficiently tight tolerances, in order to prevent partial recoherence of the long range wake due to errors.

In this paper, we have concentrated most of our discussion on controlling the fundamental transverse mode, since it is by far the most detrimental. While our work to date indicates that the other transverse HOMs and the longitudinal HOMs can be sufficiently well controlled via either of the two methods, further study of this question is continuing.

The choice of the best method is also of course dependent on the length of the bunch train. Here we have assumed that we will want to run a future linear collider with rather long bunch trains (of order a filling time in length). This places stricter requirements on the suppression of the long-range wakefields. However, the benefits of increased luminosity and greater energy efficiency are substantial.

REFERENCES

[1] International Workshop on Next-Generation Linear Colliders, Stanford Linear Accelerator Center, Stanford, California, 28 Nov–9 Dec, 1988.; SLAC–Report–335.

[2] Second International Workshop on Next-Generation Linear Colliders (LC90), KEK, Tsukuba, Japan, 28 March–5 April, 1990.; KEK 90–92.

[3] Third International Workshop on Linear Colliders (LC91), BINP, Protvino, USSR, 17–27 Sept, 1991.

[4] Fourth International Workshop on Linear Colliders (LC92), Garmisch-Partenkirschen, Germany, 25 July–2 August, 1992.

[5] R.D. Ruth, Workshop on the Physics of Linear Colliders, Capri, Italy, 1988; SLAC–PUB–4541 (unpublished).

[6] Such schemes have been suggested by R. Miller and R. Palmer.

[7] K.A. Thompson and R.D. Ruth, Proceedings of the 1993 Particle Accelerator Conference, May 17–20, 1993, Washington, D.C.; SLAC–PUB–6154.

[8] For bunch trains of intermediate length, see also Z.D. Farkas, Proceedings of 1992 Linear Accelerator Conference, Ottawa, Canada, Aug. 24–28, 1992; SLAC–PUB–5879.

[9] K.A. Thompson and J.W. Wang, Proceedings of 1991 Particle Accelerator Conference, San Francisco, Calif., May 6–9, 1991; SLAC–PUB–5465.

[10] N. Holtkamp, H.-G. Beyer, in Ref. 3.

[11] R.H. Miller, et.al., Proceedings of 15th International Conference on High Energy Accelerators, Hamburg, Germany, July 20–24, 1992; SLAC–PUB–5865.

[12] R. B. Palmer, Proceedings of DPF Summer Study, Snowmass (1988), SLAC–PUB–4542.

[13] R.B. Neal and W.H. Panofsky, Science, **152**, 1353 (1966).

[14] W.K.H. Panofsky and M. Bander, Rev.Sci.Instrum. **39**, 206 (1968).

[15] *The Stanford Two-mile Accelerator*, edited by R.B. Neal (Benjamin, New York, 1968.

[16] R.H. Helm et al., I.E.E.E. Trans. Nucl. Sci. **NS16** (1969).

[17] J. Haimson, in P.M. Lapostolle and A.L. Septier, *Linear Accelerators*, (North-Holland, Amsterdam, 1970).

[18] K.A. Thompson and R.D. Ruth, Proceedings of 1989 Particle Accelerator Conference, Chicago, March 20–23, 1989; SLAC–PUB–4873.

[19] K.A. Thompson and R.D. Ruth, Phys. Rev. D, **41**, 964 (1990).

[20] D.U.L.Yu and P.B. Wilson, presented at 14th International Conference on High Energy Accelerators, Tsukuba, Japan, Aug. 22–26, 1989; SLAC–PUB–5062; published in Part.Accel. **30**, 65–72, 1990.

[21] H. Deruyter, et.al., Proceedings of 1990 Linear Accelerator Conference, Albuquerque, New Mexico, Sept. 10–14, 1990.

[22] D. Yu and J.S. Kim, Proceedings of 1991 Particle Accelerator Conference, San Francisco, Calif., May 6–9, 1991.

[23] T. Higo, M. Takao, K. Kubo, and K. Takata, Proceedings of 1991 Particle Accelerator Conference, San Francisco, Calif., May 6–9, 1991.

[24] K.L.F. Bane and R.L. Gluckstern, to be published.

[25] T. Weiland, Nucl.Instr.Meth., **212**, 13 (1983).

[26] Y. Goren and D.U.L. Yu, Proceedings of 1989 Particle Accelerator Conference, Chicago, Illinois, March 20–23, 1989.

[27] Norman M. Kroll and David U.L.Yu, Part. Accel. **34**, 231 (1990); SLAC–PUB–5171.

[28] H. Deruyter, et.al., Proceedings of 1989 Particle Accelerator Conference, Chicago, Illinois, March 20–23, 1989; SLAC–PUB–4865.

[29] H. Deruyter, et.al., 2nd European Particle Accel. Conf., Nice, France, June 12–16, 1990; SLAC–PUB–5263.

[30] See T.Weiland, in *Frontiers of Particle Beams: Intensity Limitations*, Proceedings, Hilton Head Island, South Carolina, USA, 7–14 Nov. 1990, (Springer-Verlag Lecture Notes in Physics, **400**, 1992), and references therein.

[31] Norman M. Kroll and Xin-Tian Lin, Proceedings of 1990 Linear Accelerator Conference, Albuquerque, New Mexico, Sept. 10–14, 1990; SLAC–PUB–5345.

[32] J. C. Slater, Microwave Electronics (Van Nostrand, New York, 1950) (Bell Telephone Laboratory Series) Ch.5 Section 1.

[33] G. Conciauro and P. Arcioni, Proceedings of the 2nd European Particle Accelerator Conference, Nice, France (1990), p 149.

[34] Norman M. Kroll and Robert Rimmer, Proceedings of IEEE Particle Accelerator Conference, San Francisco, California, May 6–9, 1991.

[35] D.U.L. Yu and N. Kroll, Proceedings of IEEE Particle Accelerator Conference, San Francisco, May 6–9, 1991.

[36] N. Kroll and X-T. Lin, Persistent Wakefields Associated with Waveguide Damping of Higher Order Modes, Proceedings of the 1993 Particle Accelerator Conference, May 17–20, 1993, Washington D.C.; SLAC–PUB–6144. The beam blow up estimates in the final paragraph of this paper have been revised downward by a substantial amount, and otherwise practical scenarios for which the effect gives rise to unacceptable beam instability have not been identified.

[37] K.L.F. Bane and R.L. Gluckstern, submitted to Particle Accelerators; SLAC–PUB–5783.

[38] J.W. Wang and B.W. Littmann, SLAC/AP–92 (September, 1991).

[39] K.Bane and B.Zotter, Proceedings of 11th International Conference on High Energy Accelerators, Geneva, (1980).

[40] T.Weiland, Nucl. Instrum. Methods **216**, 329 (1983).

[41] K. Halbach and R.F. Holsinger, Particle Accelerators, Vol.7, 1976.

[42] E.M.Nelson, Proceedings of 1992 Linear Accelerator Conference, Ottawa, Canada, Aug. 24–28, 1992; SLAC–PUB–5881.

[43] M. Drevlak, Thesis, Technische Hochschule Darmstadt, Darmstadt, Germany, December 1991.

[44] K. Bane and N. Holtkamp, SLAC–AAS–63, September 1991.

[45] M. Yamamoto, *et.al.*, KEK–PREPRINT–91–153, November 1991.

[46] J.M.Paterson, et.al., Proceedings of 15th International Conference on High Energy Accelerators, Hamburg, Germany, July 20–24, 1992; SLAC–PUB–5928.

[47] "Next Linear Collider Test Accelerator Conceptual Design Report", SLAC–REPORT–411 (1993).

[48] K.L.F. Bane, in *Physics of Particle Accelerators*, edited by M. Month and M. Dienes (AIP Conf. Proc. No. 153) (AIP, New York, 1987).

[49] K.A. Thompson, unpublished.

[50] C. Adolphsen, presented at 15th International Conference on High-Energy Accelerators, Hamburg, Germany, July 20–24, 1992; SLAC–PUB–5942.

[51] K. Thompson, C. Adolphsen, and K. Bane, Proceedings of the 1993 Particle Accelerator Conference, May 17–20, 1993, Washington, D.C.; SLAC–PUB–6153.

[52] M. Yamamoto, et.al., Proceedings of 1992 Linear Accelerator Conference, Ottawa, Canada, 24–28 August, 1992.

[53] S.A. Heifets and S.A. Kheifets, submitted to IEEE Trans. on Microwave Theory and Techniques; SLAC–PUB–5907.

FIGURE CAPTIONS

1) Field patterns of HEM mode: (a) electric field lines in longitudinal cross-section of three cells in a disk-loaded structure, (b) magnetic field lines in transverse cross-section through center of a cell.

2) Example of structure with radial slots in iris.

3) Example of structure with circumferential-slot coupling: crossed-waveguide structure, with two half-cells and one full cell.

4) Schematic cross section of cells, (a) in simplified structure (square corners and fixed disk thickness), (b) in actual structure.

5) Three dimensional plot of the accelerating (TM_{01}) and dipole (TM_{11}) mode frequencies with dependence on iris diameter $2a$ and cavity diameter $2b$, for simplified detuned structure of Fig. 4(a).

6) a, b pairs with the accelerating mode frequency $f_{rf} = 11.424$ GHz and phase advance $\phi = 2\pi/3$, for simplified detuned structure of Fig. 4(a).

7) Dipole mode frequency dependence on iris radius a, for simplified detuned structure of Fig. 4(a).

8) Quality factor Q along the simplified detuned structure.

9) Group velocity v_g/c for the accelerating mode along the simplified detuned structure.

10) Shunt impedance $r(s)$ of the simplified detuned structure.

11) Accelerating electric field $E_z(s)$ along the axis of the simplified detuned structure. Conventional constant-impedance and constant-gradient structures with the same input power and attenuation are also shown.

12) Energy gain $U(s)$ due to accelerating voltage on the axis of the simplified detuned structure.

13) Dispersion curves of TM_{01} modes, for the simplified detuned structure.

14) Dispersion curves of dipole modes, for the simplified detuned structure.

15) Group velocity v_g/c of the first dipole mode along the simplified detuned structure.

16) Accelerating electric field $E_z(s)$ along the axis of the actual NLC test structure (which has varying disk thickness and rounded iris corners). The field for conventional constant-impedance and constant-gradient structures with the same input power and attenuation as the detuned structure are also shown.

17) The envelope $\hat{W}$ of the wake function as a function of $z = ct$, calculated using the uncoupled model.

18) Results of single-band coupled model: (a) the mode spectrum, (b) the kick factor, (c) the mode density (normalized so that the integral of dn/df is one), and (d) the product of kick factor and mode density. Dashed lines show the results of the uncoupled model for comparison.

19) The envelope of the wake function calculated using the single-band, coupled model.

20) The double-band circuit solutions for a structure with six identical cells (located by the plotting symbols). Results are given for seven cell geometries. The solid circles represent modes belonging to the first band, the open circles represent those of the second band. For comparison, the dispersion curves obtained from TRANSVRS are also shown. The dots give the speed of light line.

21) Results of double-band coupled model: (a) the mode spectrum, (b) the kick factor, (c) the mode density (normalized so that the integral of dn/df over the first half of the modes is one), and (d) the product of kick factor and mode density. Dashed lines show the results of the uncoupled model for comparison.

22) The envelope of the wake function calculated using the double-band, coupled model.

23) Mechanical design of 1.8-meter detuned structure.

24) Mechanical design of cells of accelerating structure.

25) (a) Value of the wake function $W(z)$ at multiples of the bunch spacing (16 rf wavelengths $\approx$ 42 cm), (b) the sum of the wake functions from the preceding $n-1$ bunches, at each bunch n, and (c) the resulting maximum beam blow-up factor x/x_0 (normalized to remove the adiabatic damping factor). The coupled wakefield of Fig. 22 is assumed.

26) The envelope of the wake function averaged over four detuned section types having interleaved frequency distributions (no frequency errors included). The coupled, double-band model was used.

27) (a) Value of the averaged (over four structure types) wake function $W(z)$ at multiples of the bunch spacing (16 rf wavelengths $\approx$ 42 cm), (b) the sum of the wake functions from the preceding $n-1$ bunches, at each bunch n, and (c) the resulting maximum beam blow-up factor x/x_0 (normalized to remove the adiabatic damping factor). The four interleaved structure types used to generate Fig. 26 have been cycled through in this simulation.

28) Beam blow-up factor x/x_0 for case of single detuned section type, including random errors with $\sigma_{e,ran} = 1 \times 10^{-4}$ and systematic errors with $\sigma_{e,sys} = 3 \times 10^{-5}$.

29) Beam blow-up factor x/x_0 for case of four detuned section types with interleaved frequency distributions, including random errors with $\sigma_{e,ran} = 1 \times 10^{-4}$ and systematic errors with $\sigma_{e,sys} = 3 \times 10^{-5}$.

30) Tolerance (in μm) of rms misalignments for 25% emittance growth (w.r.t. beam centroid) of the multibunch beam as a function of number of cells i_m per uniformly misaligned piece of structure. One hundred seventy four different random distributions were calculated at each value of i_m. The error bars show the rms on each side of the mean (circles). The squares and triangles show the points for which 10% and 5%, respectively, of the distributions give a tighter tolerance.

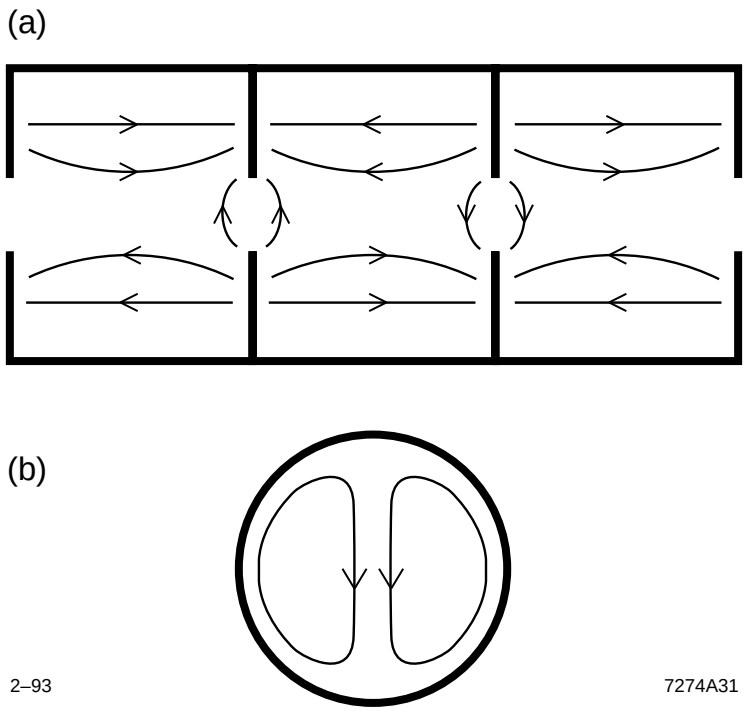

Fig. 1

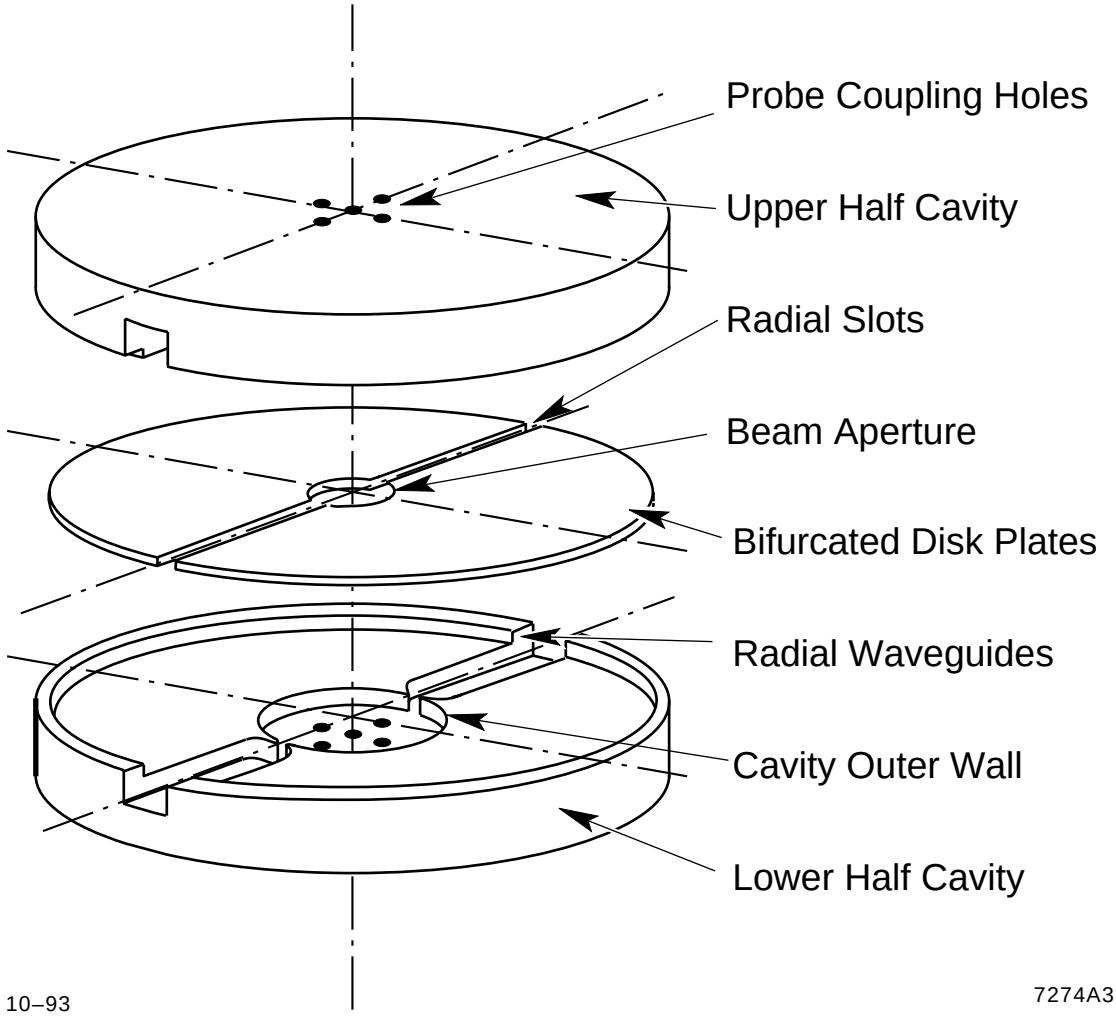
Probe Coupling Holes
Upper Half Cavity
Radial Slots
Beam Aperture
Bifurcated Disk Plates
Radial Waveguides
Cavity Outer Wall
Lower Half Cavity
10–93
7274A3

Fig. 2

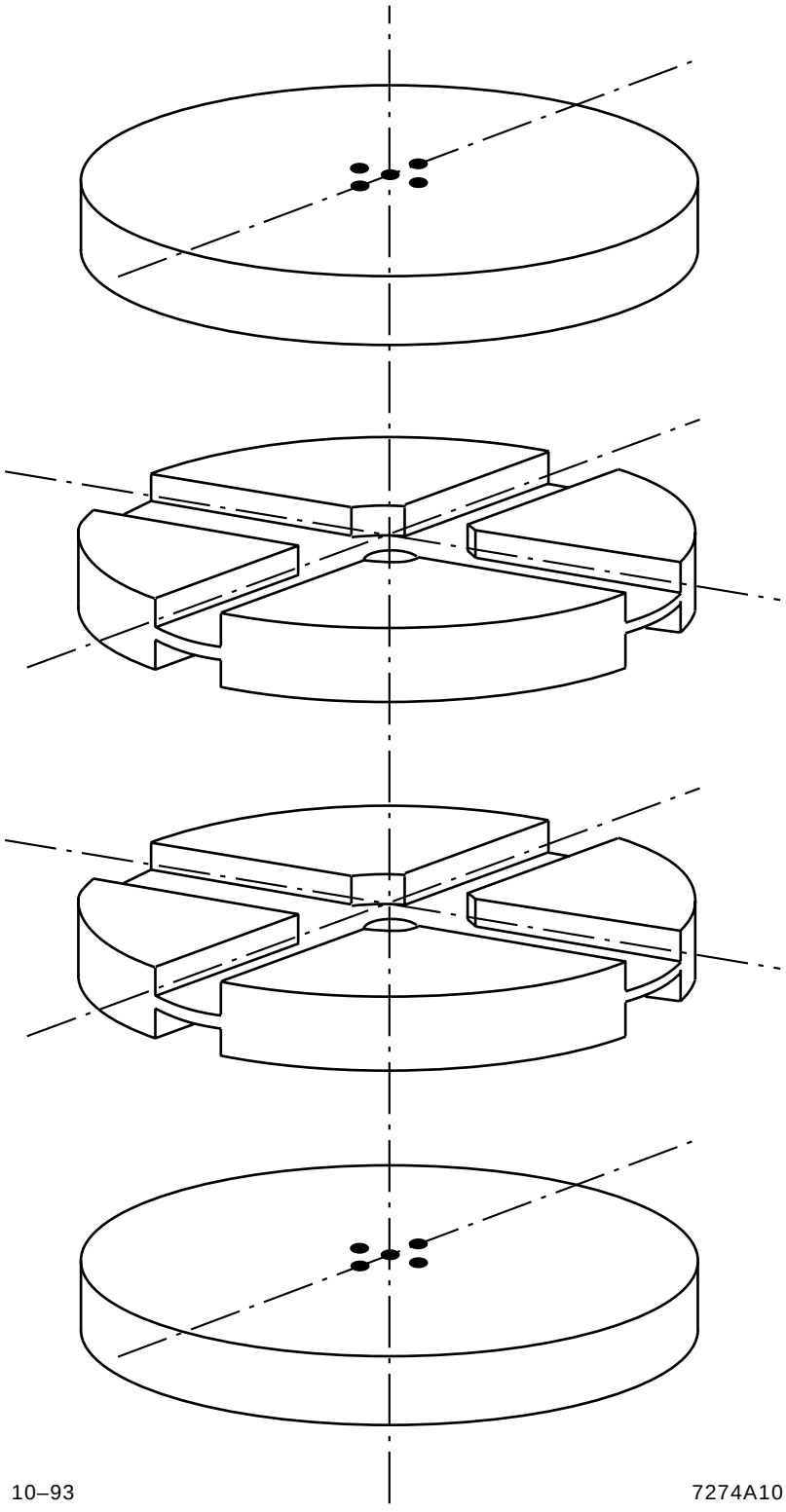

Fig. 3

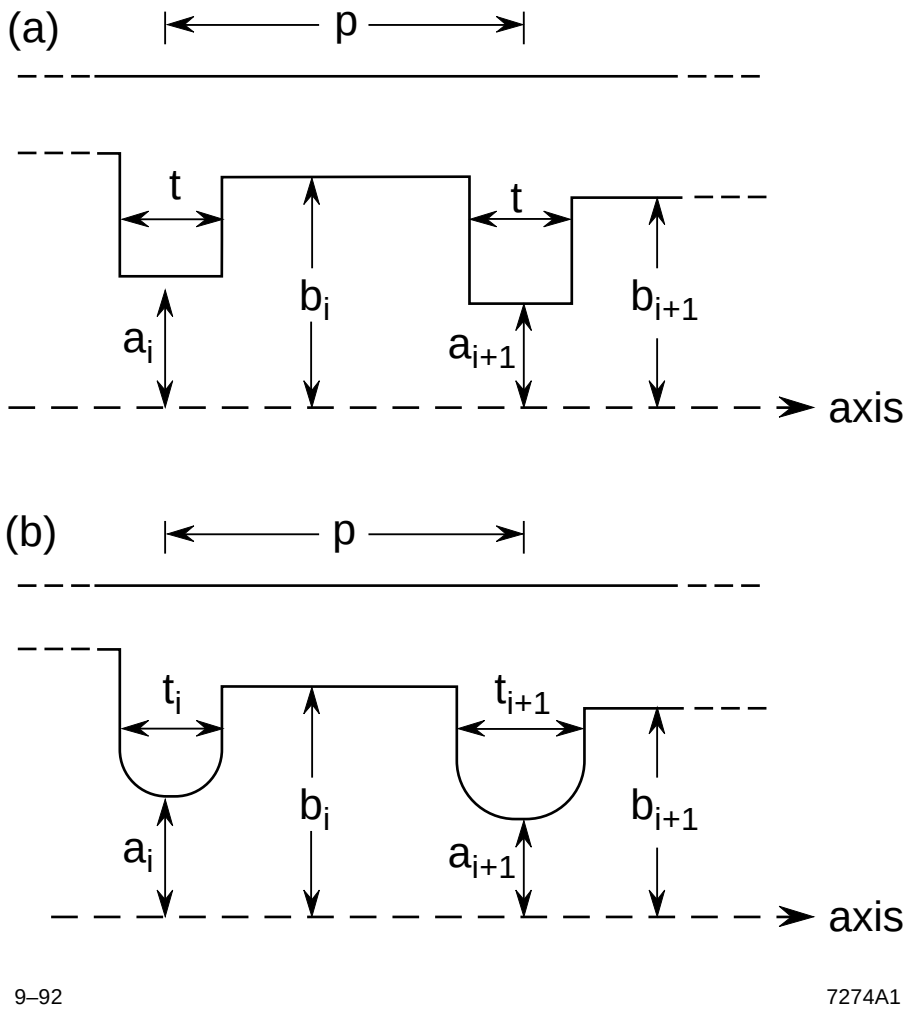

Fig. 4

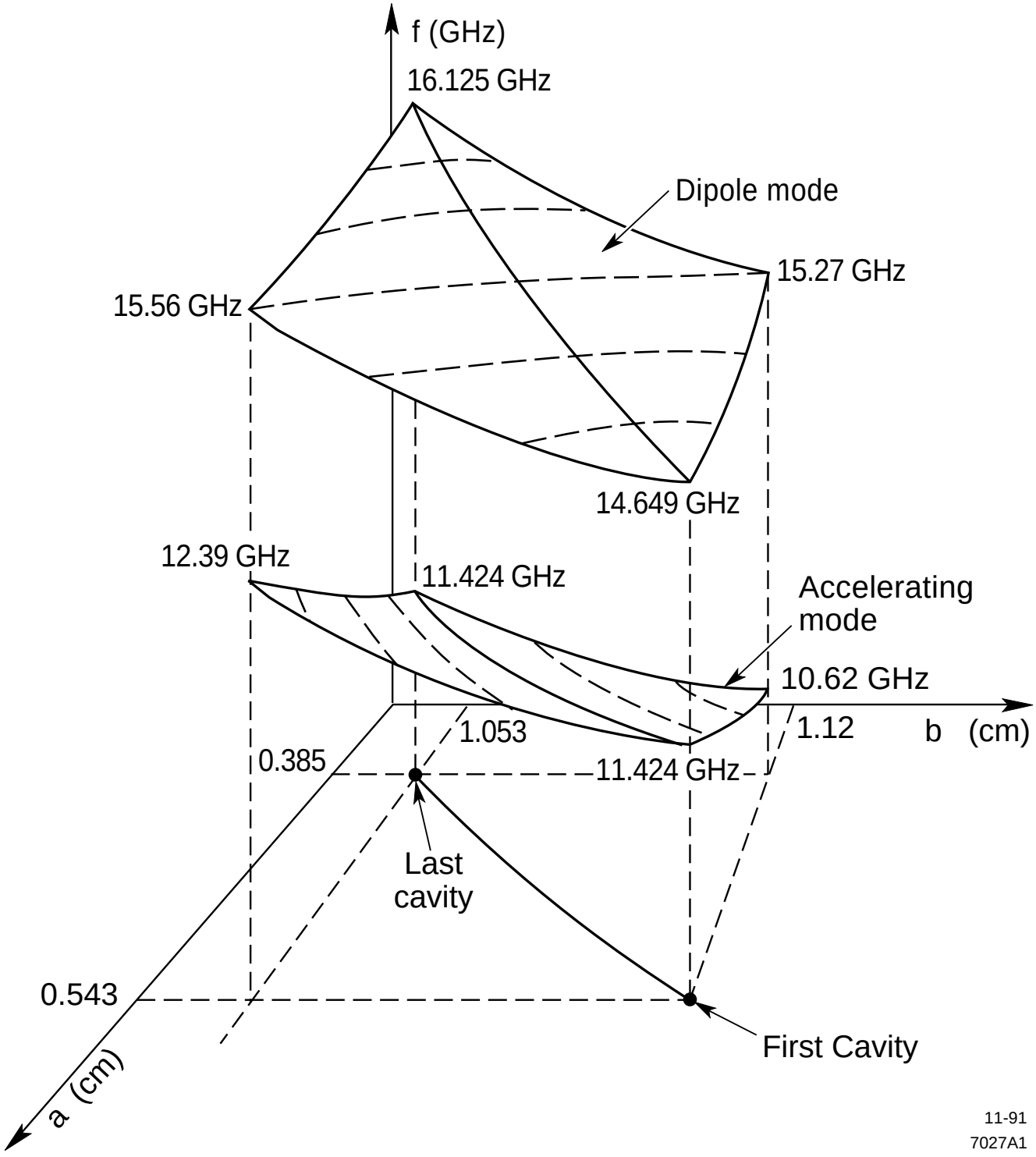
f (GHz)
16.125 GHz
Dipole mode
15.27 GHz
15.56 GHz
14.649 GHz
12.39 GHz
11.424 GHz
Accelerating
mode
10.62 GHz
1.053
1.12
b (cm)
0.385
11.424 GHz
Last
cavity
0.543
First Cavity
a (cm)
11-91
7027A1

Fig. 5

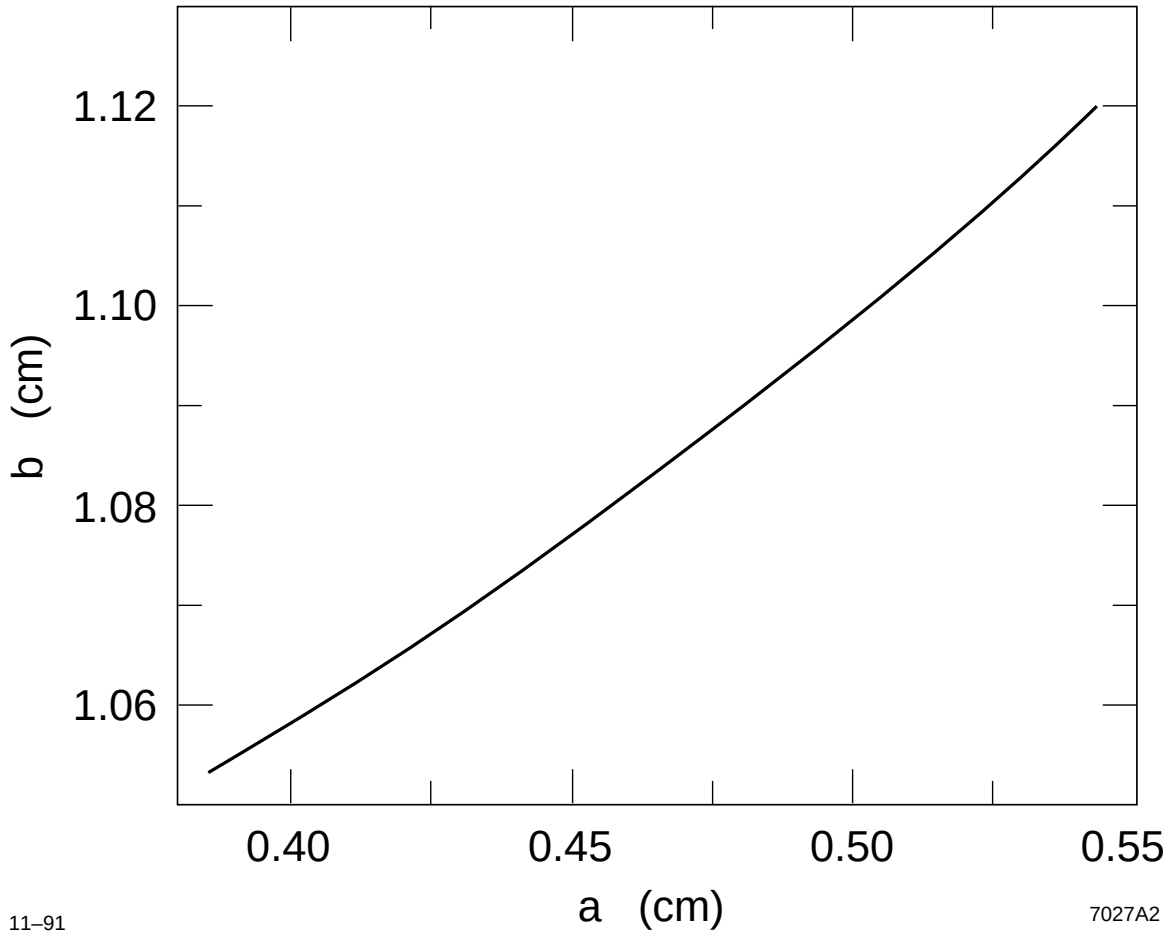

Fig. 6

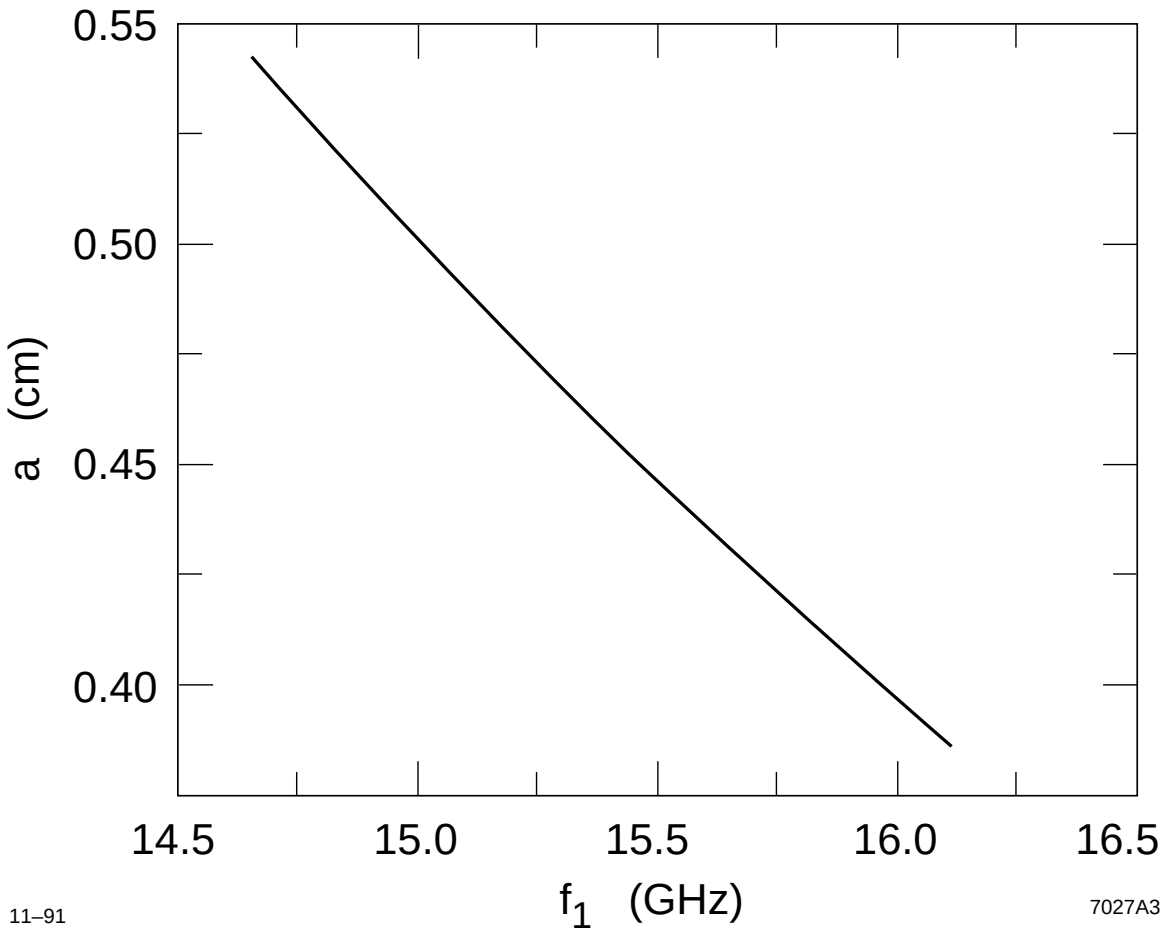

Fig. 7

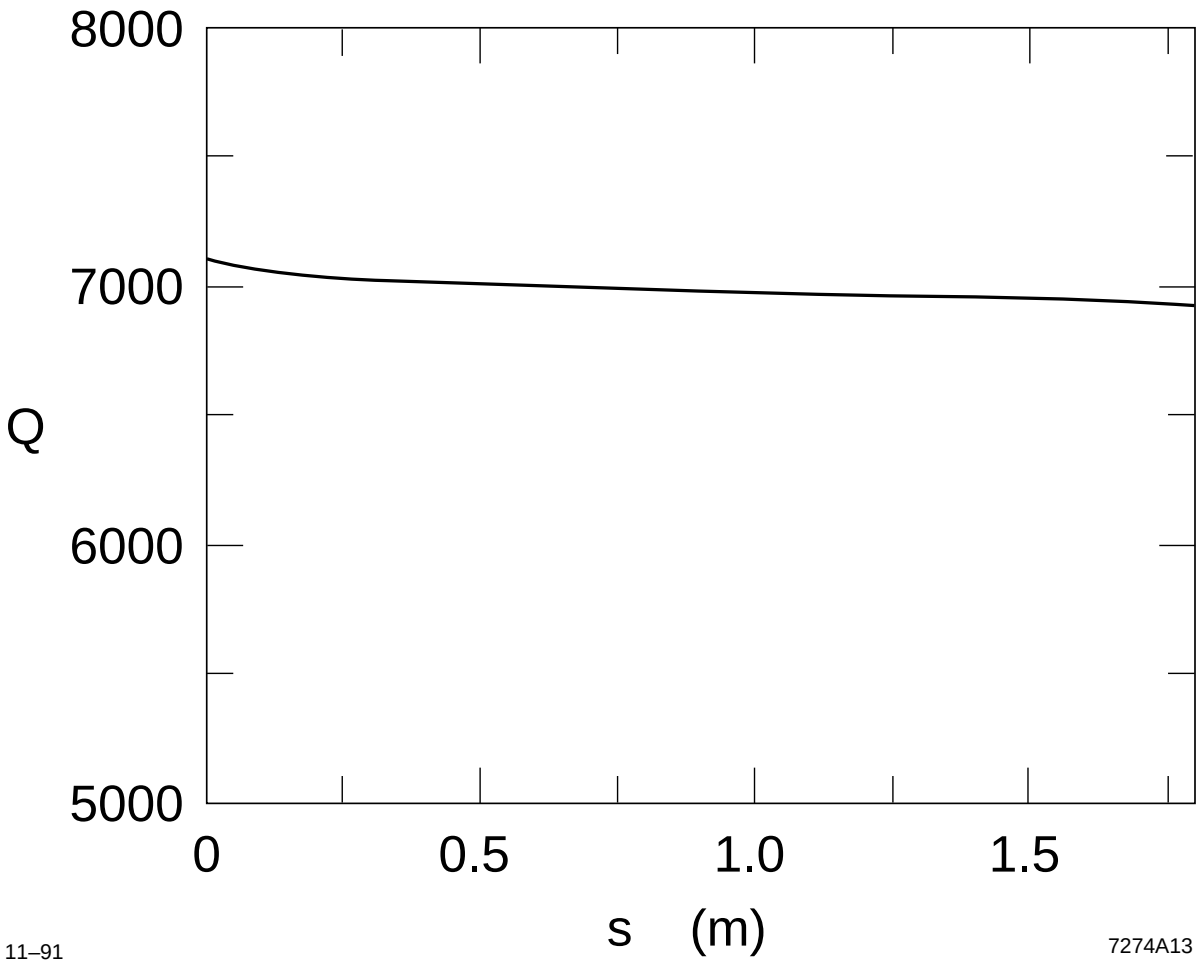

Fig. 8

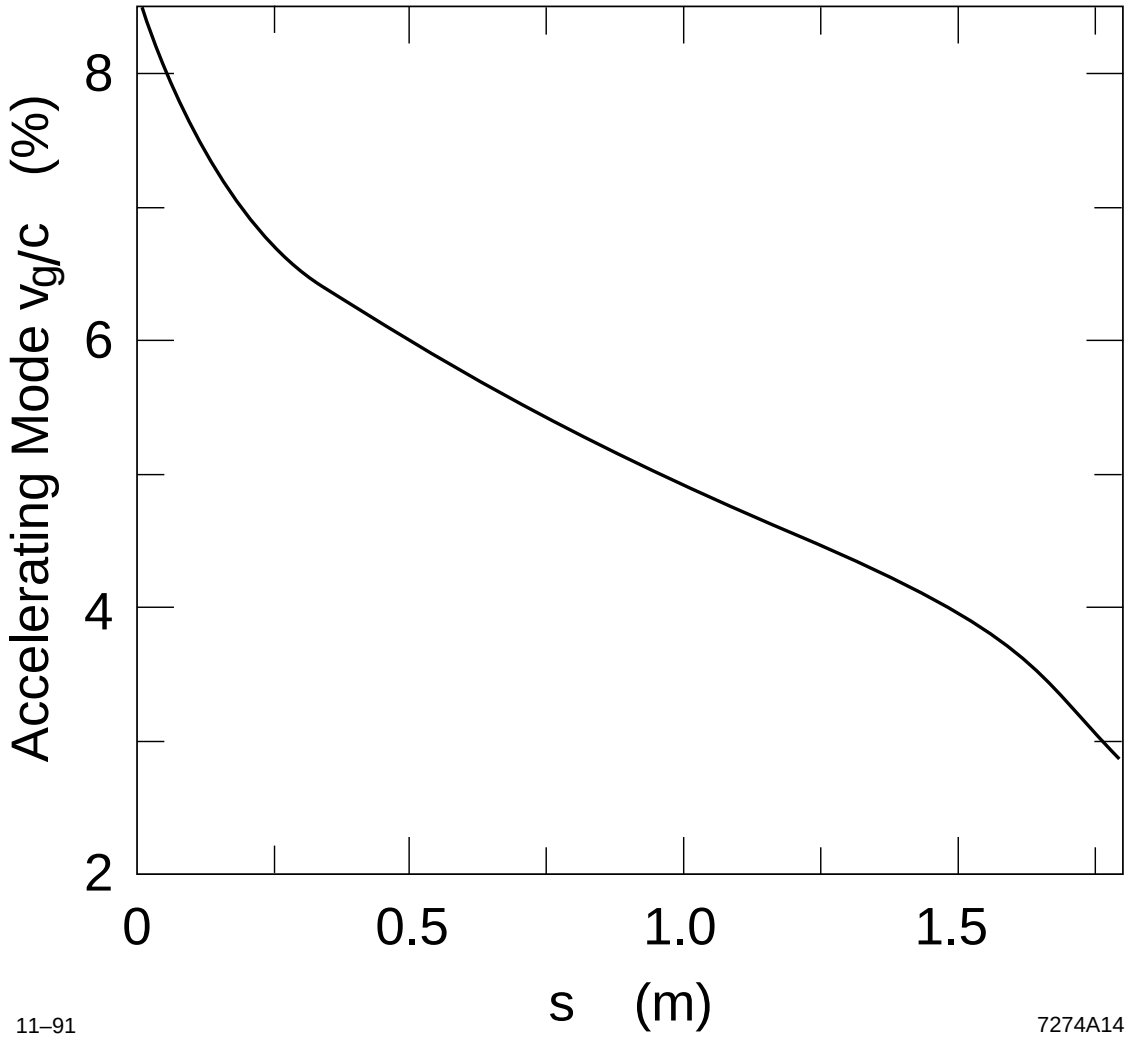

Fig. 9

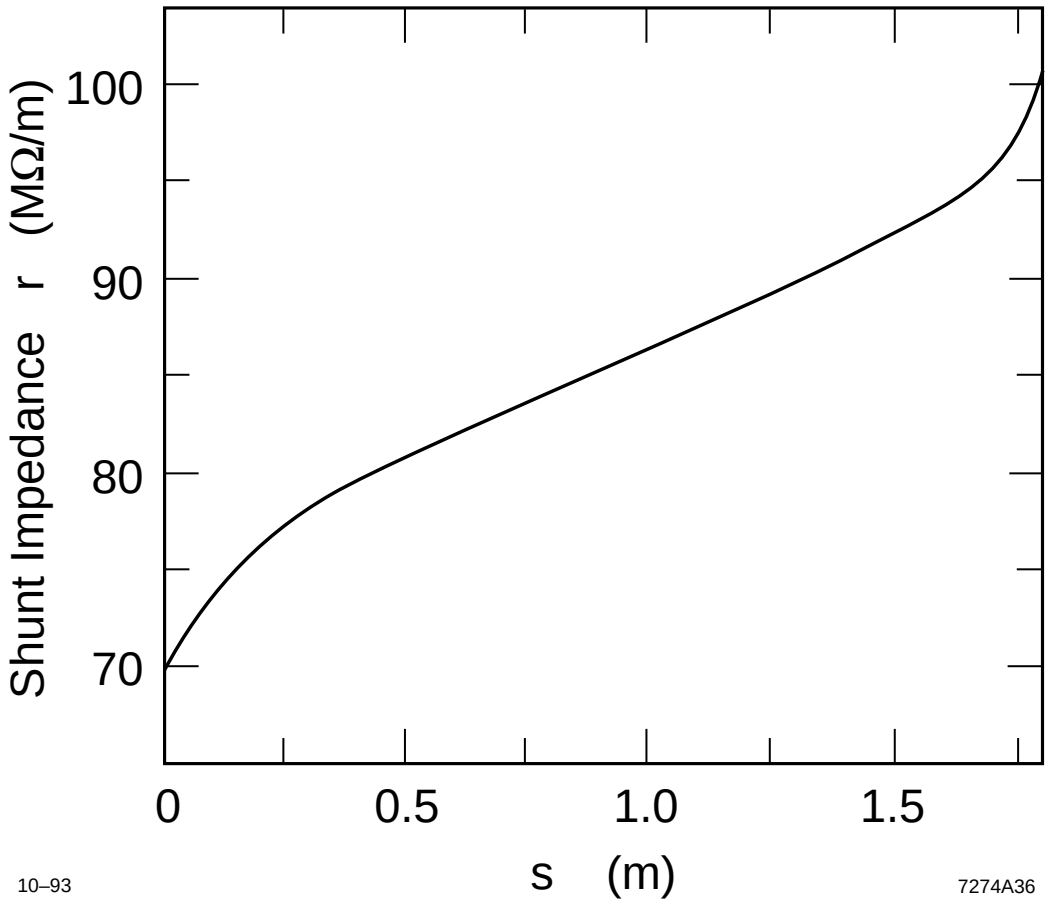

Fig. 10

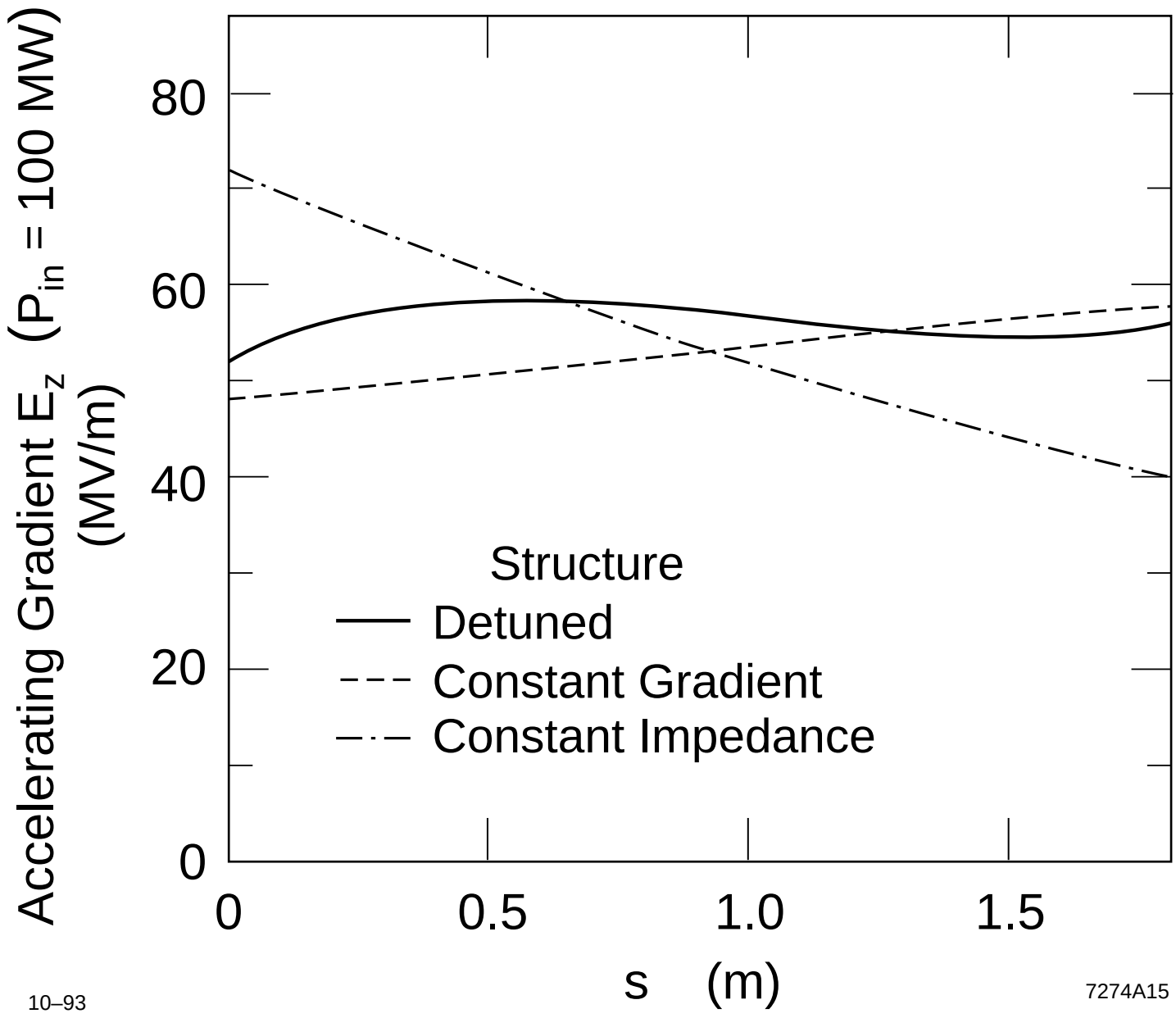
Accelerating Gradient E_z (P_{in} = 100 MW) (MV/m)
80
60
40
20
0
0
0.5
1.0
1.5
s (m)
Structure
Detuned
Constant Gradient
Constant Impedance
10–93
7274A15

Fig. 11

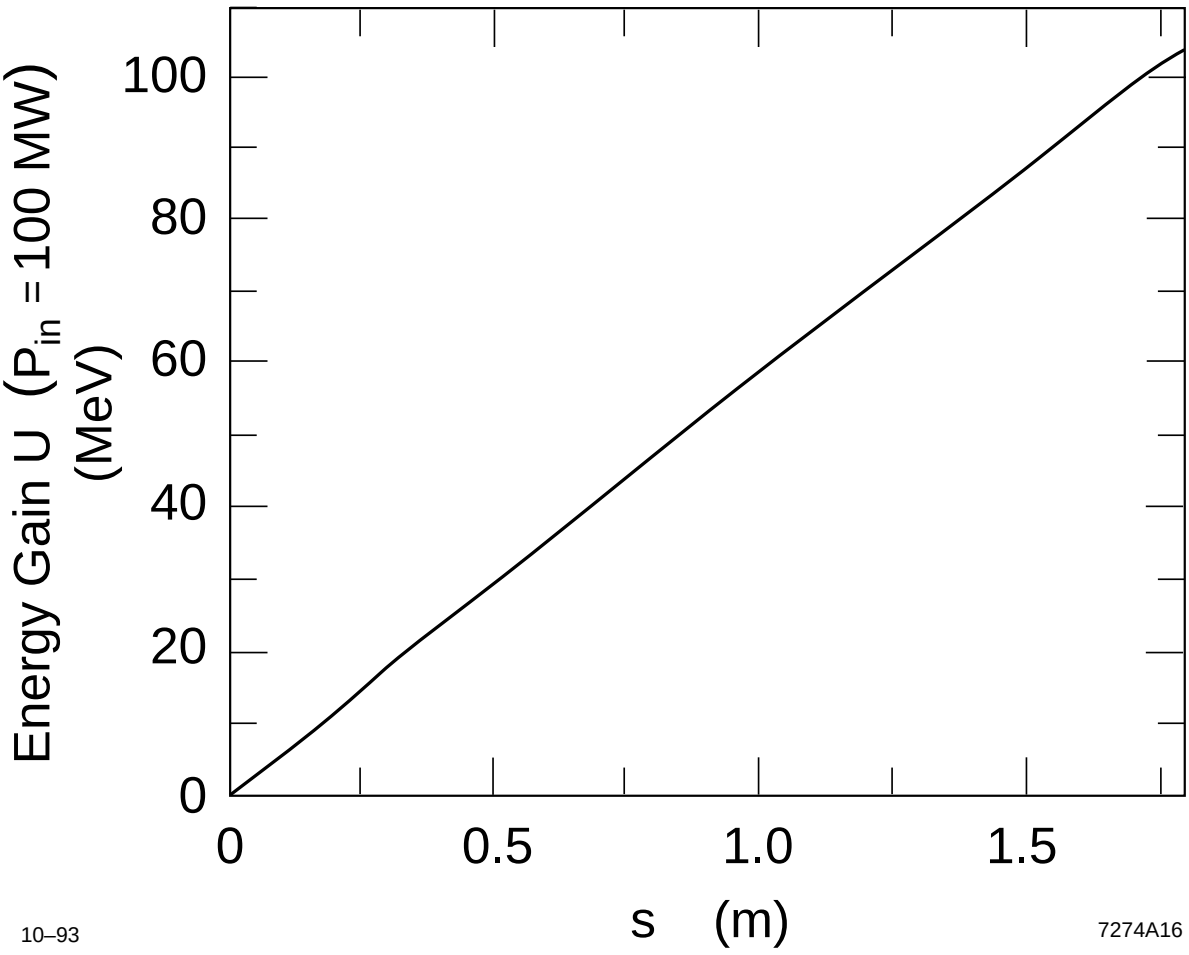
Energy Gain U (P_in = 100 MW)
(MeV)
100
80
60
40
20
0
0
0.5
1.0
1.5
s (m)
10–93
7274A16

Fig. 12

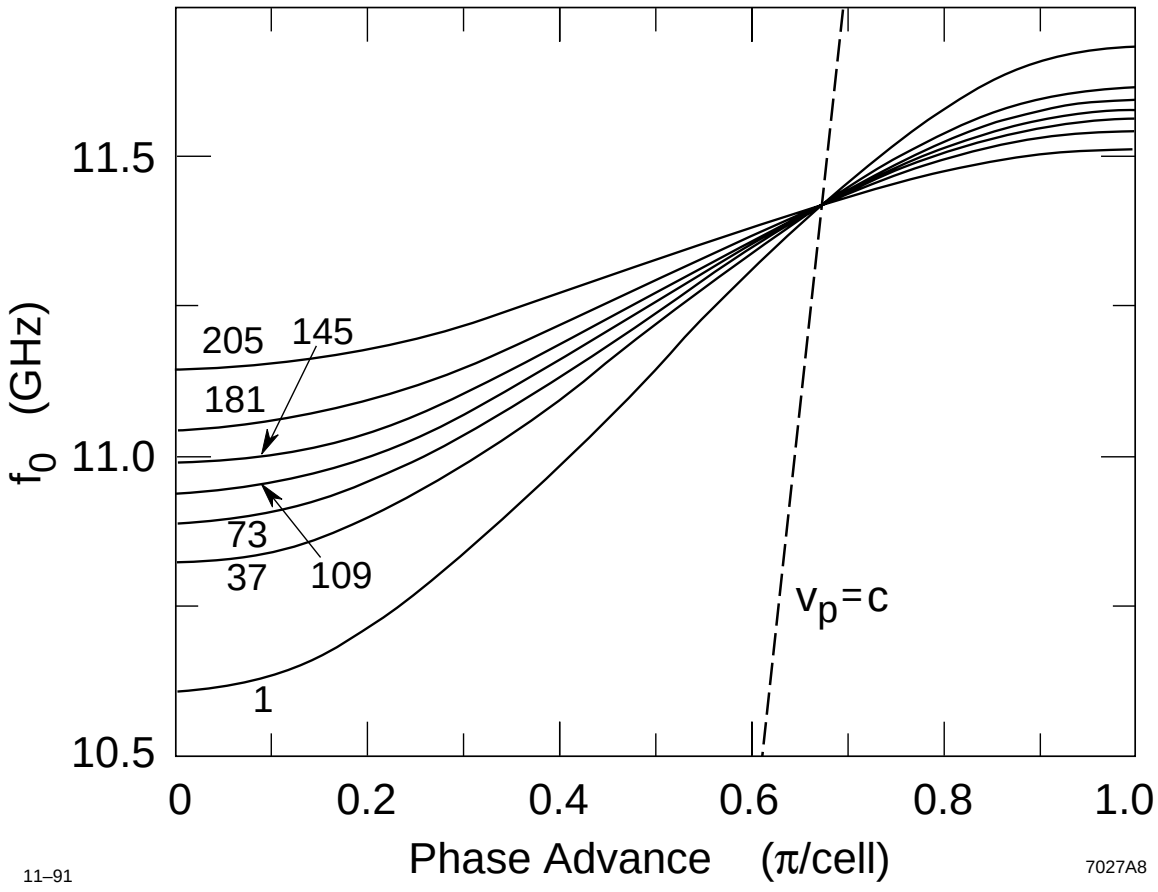
11.5
11.0
10.5
f_0 (GHz)
205
145
181
73
37
109
1
$v_p = c$
0
0.2
0.4
0.6
0.8
1.0
Phase Advance (π/cell)
11–91
7027A8

Fig. 13

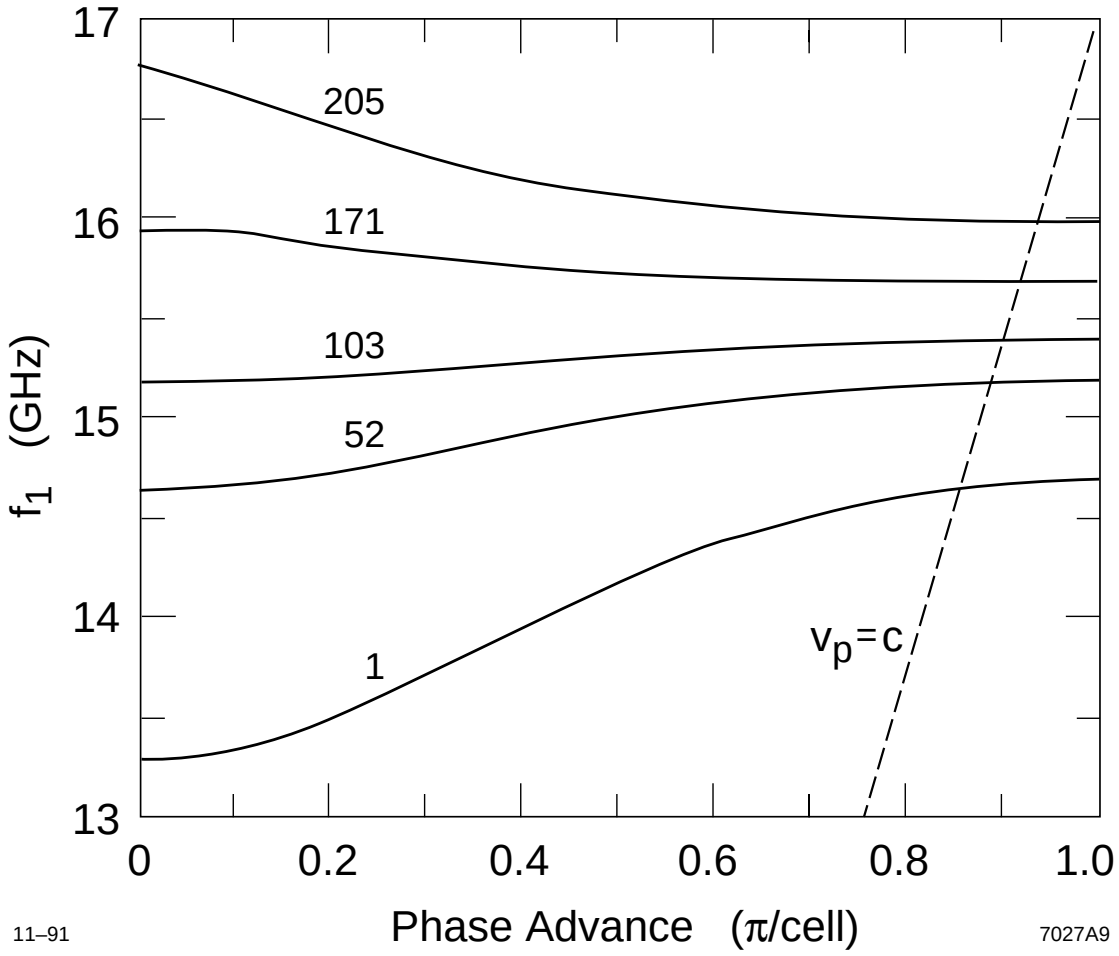
17
16
15
14
13
0
0.2
0.4
0.6
0.8
1.0
205
171
103
52
1
$v_p = c$
f_1 (GHz)
Phase Advance (π/cell)
11–91
7027A9

Fig. 14

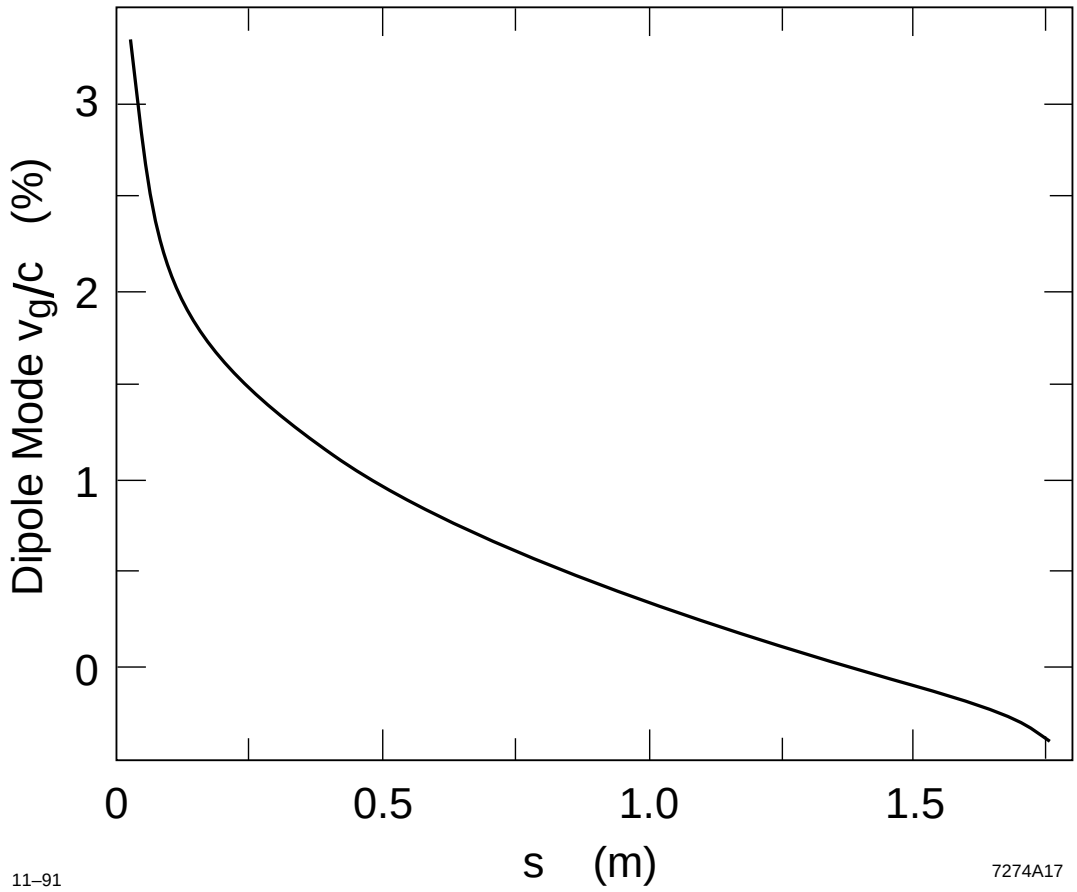

Fig. 15

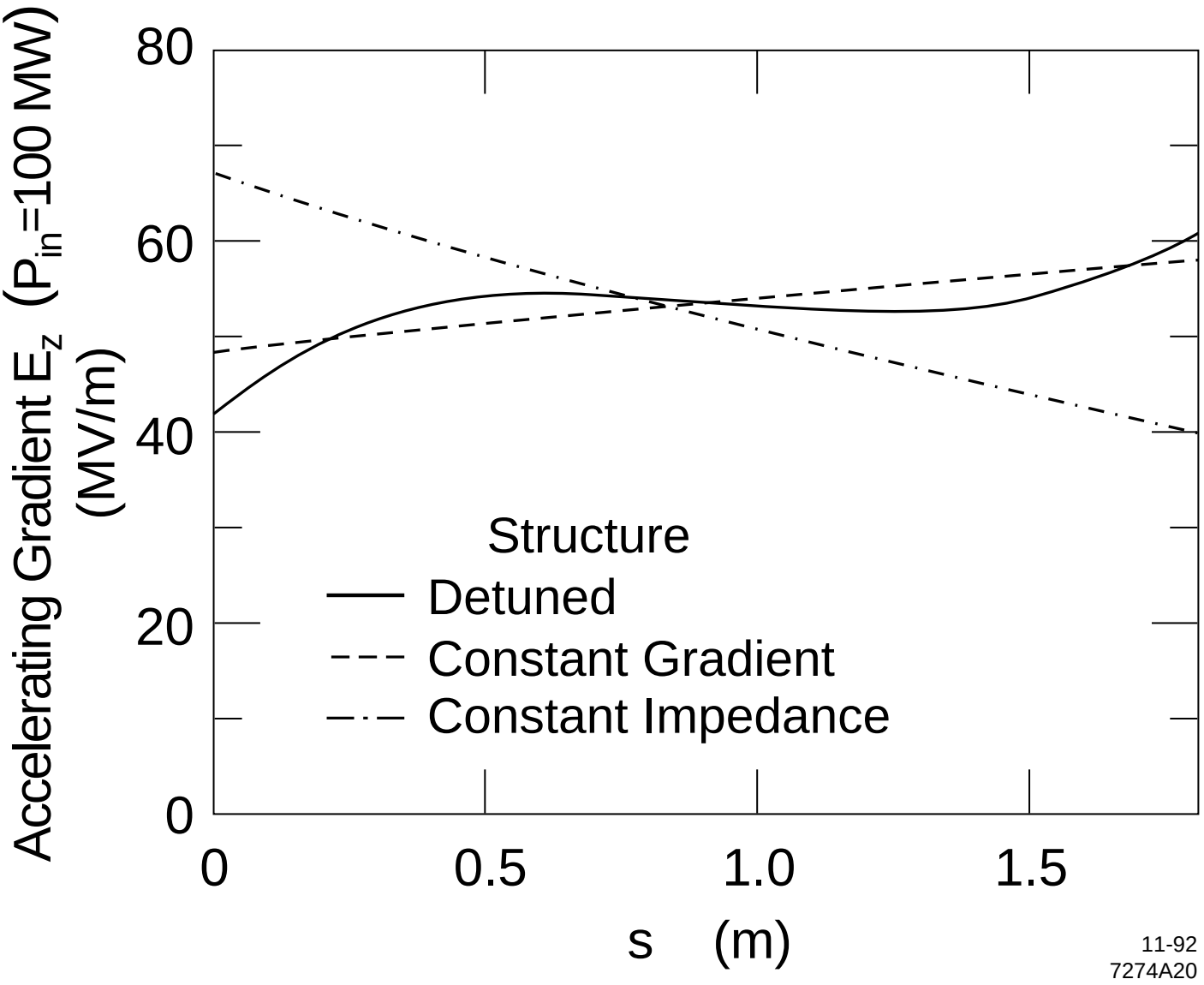
Accelerating Gradient E_z (P_{in}=100 MW)
(MV/m)
80
60
40
20
0
0
0.5
1.0
1.5
s (m)
Structure
Detuned
Constant Gradient
Constant Impedance
11-92
7274A20

Fig. 16

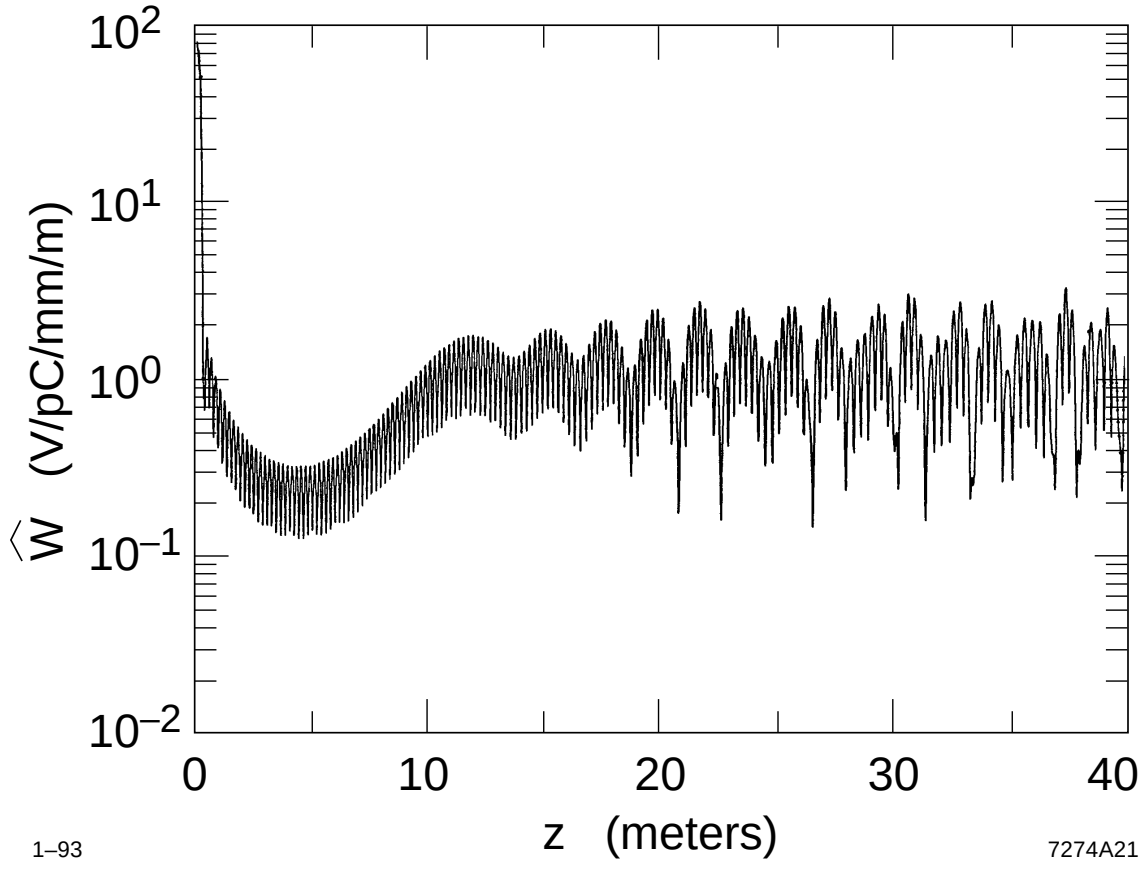
10^2
10^1
10^0
10^{-1}
10^{-2}
$\langle W \rangle$ (V/pC/mm/m)
0
10
20
30
40
z (meters)
1–93
7274A21

Fig. 17

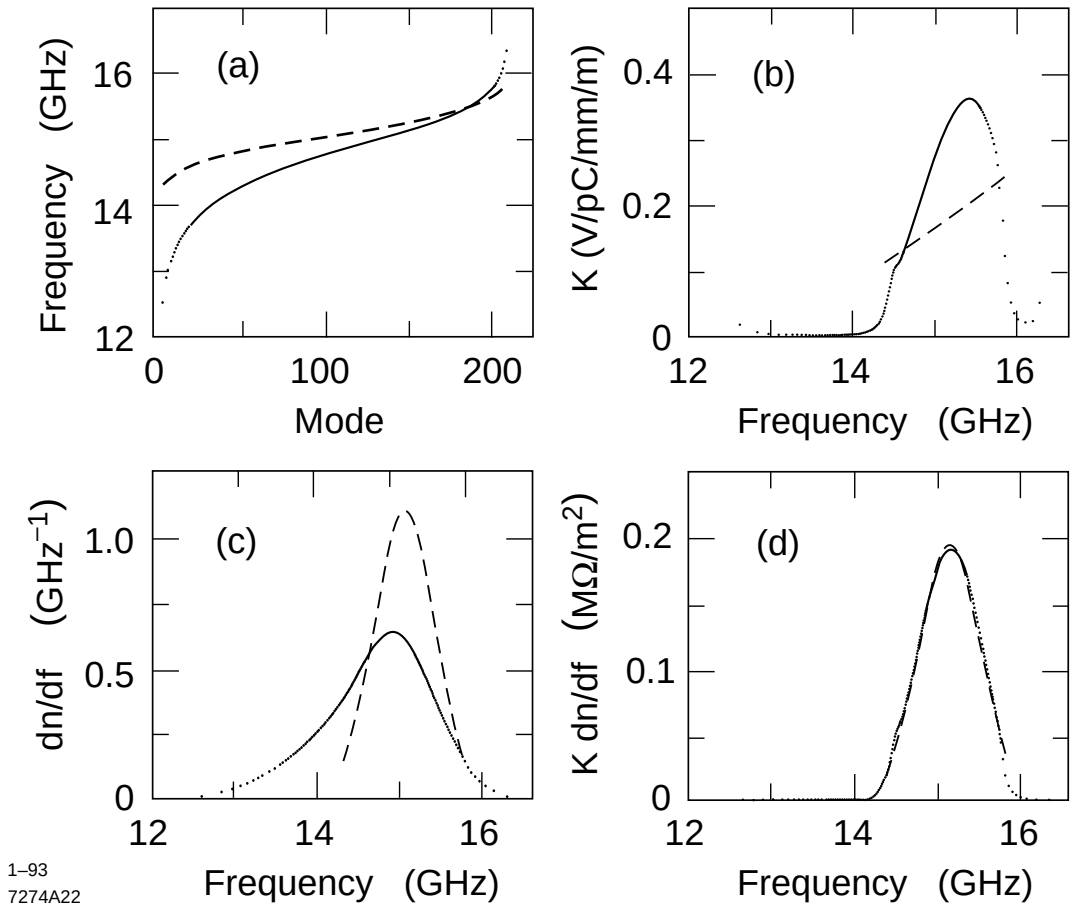
(a)
Frequency (GHz)
16
14
12
0
100
200
Mode
(b)
K (V/pC/mm/m)
0.4
0.2
0
12
14
16
Frequency (GHz)
(c)
dn/df (GHz^{-1})
1.0
0.5
0
12
14
16
Frequency (GHz)
(d)
K dn/df (MΩ/m^2)
0.2
0.1
0
12
14
16
Frequency (GHz)
1–93
7274A22

Fig. 18

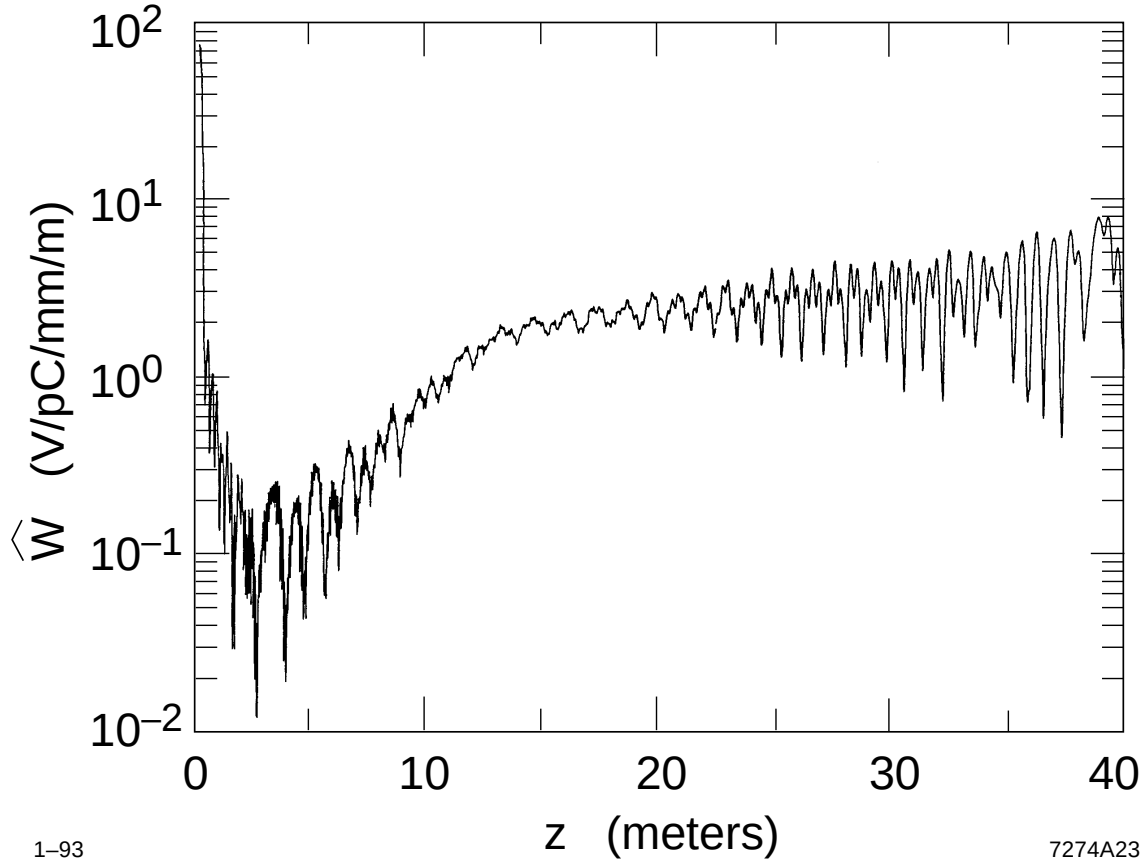
10^2
10^1
10^0
10^{-1}
10^{-2}
$\langle W \rangle$ (V/pC/mm/m)
0
10
20
30
40
z (meters)
1–93
7274A23

Fig. 19

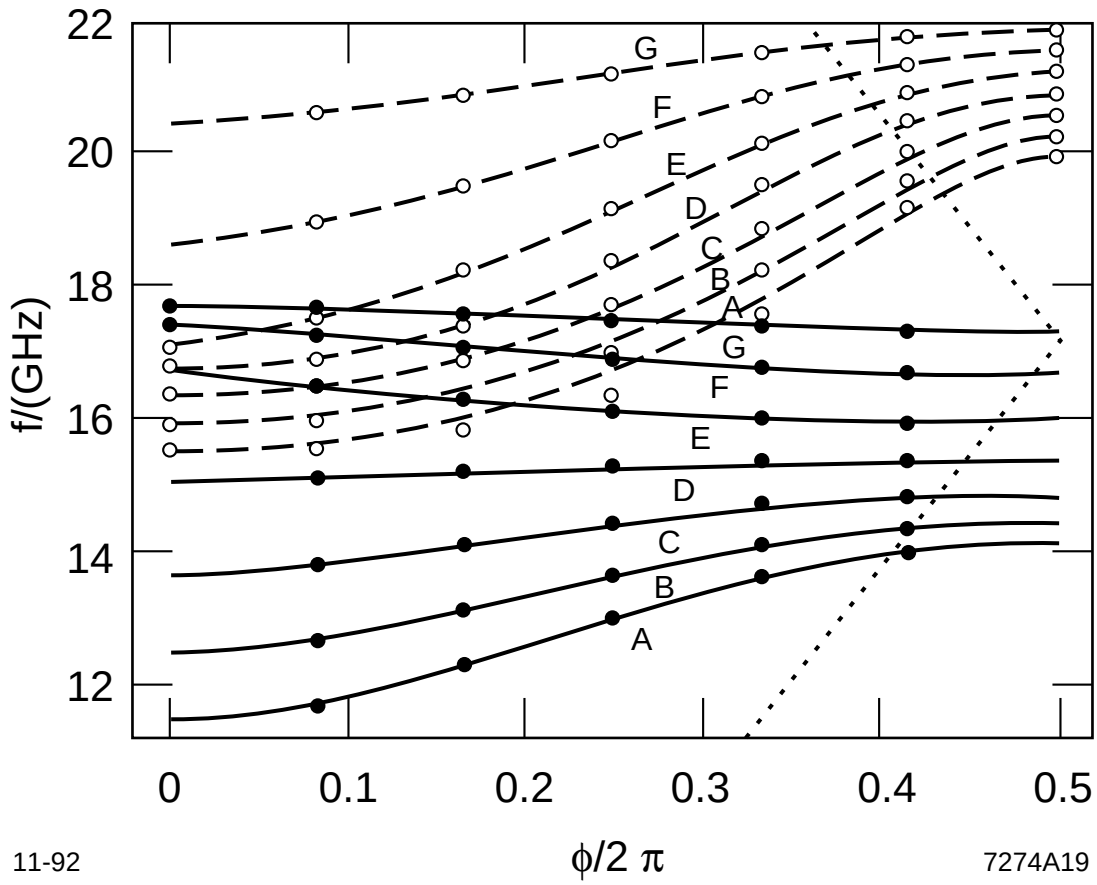

Fig. 20

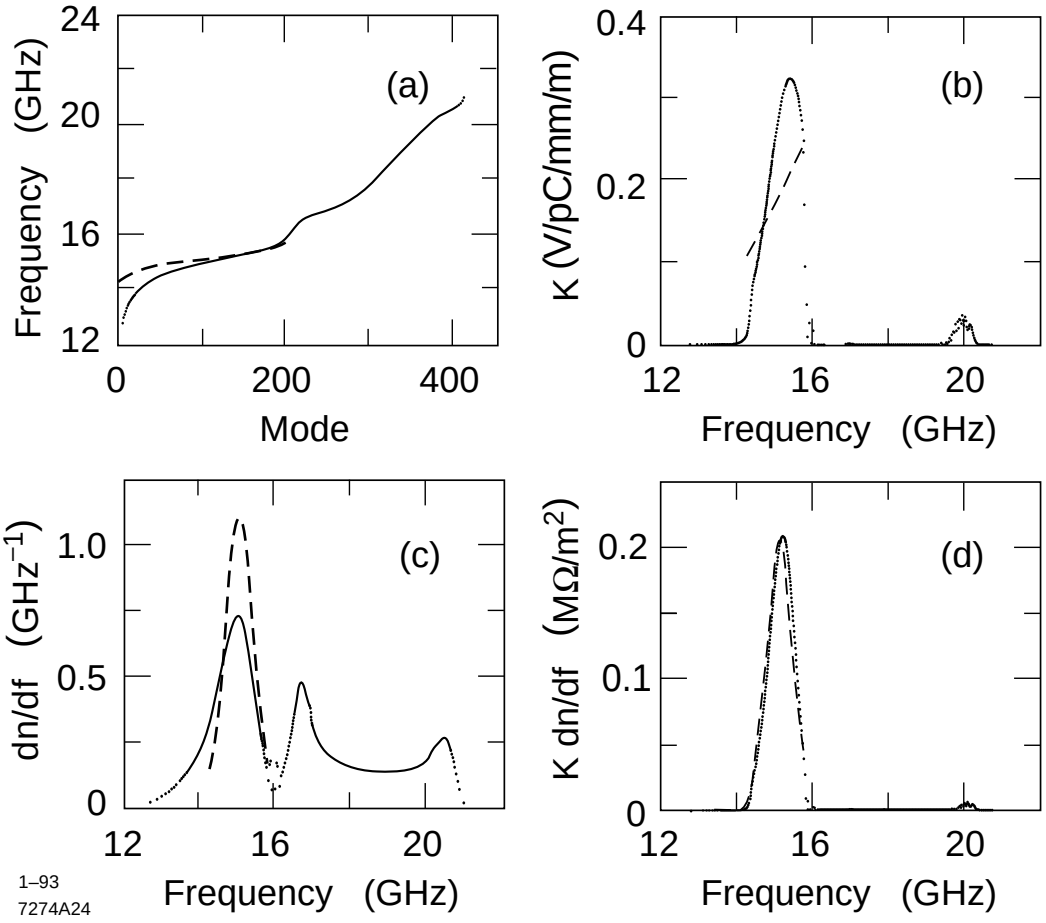
(a)
Frequency (GHz)
24
20
16
12
0
200
400
Mode
(b)
κ (V/pC/mm/m)
0.4
0.2
0
12
16
20
Frequency (GHz)
(c)
dn/df (GHz^{-1})
1.0
0.5
0
12
16
20
Frequency (GHz)
(d)
κ dn/df (MΩ/m^2)
0.2
0.1
0
12
16
20
Frequency (GHz)
1–93
7274A24

Fig. 21

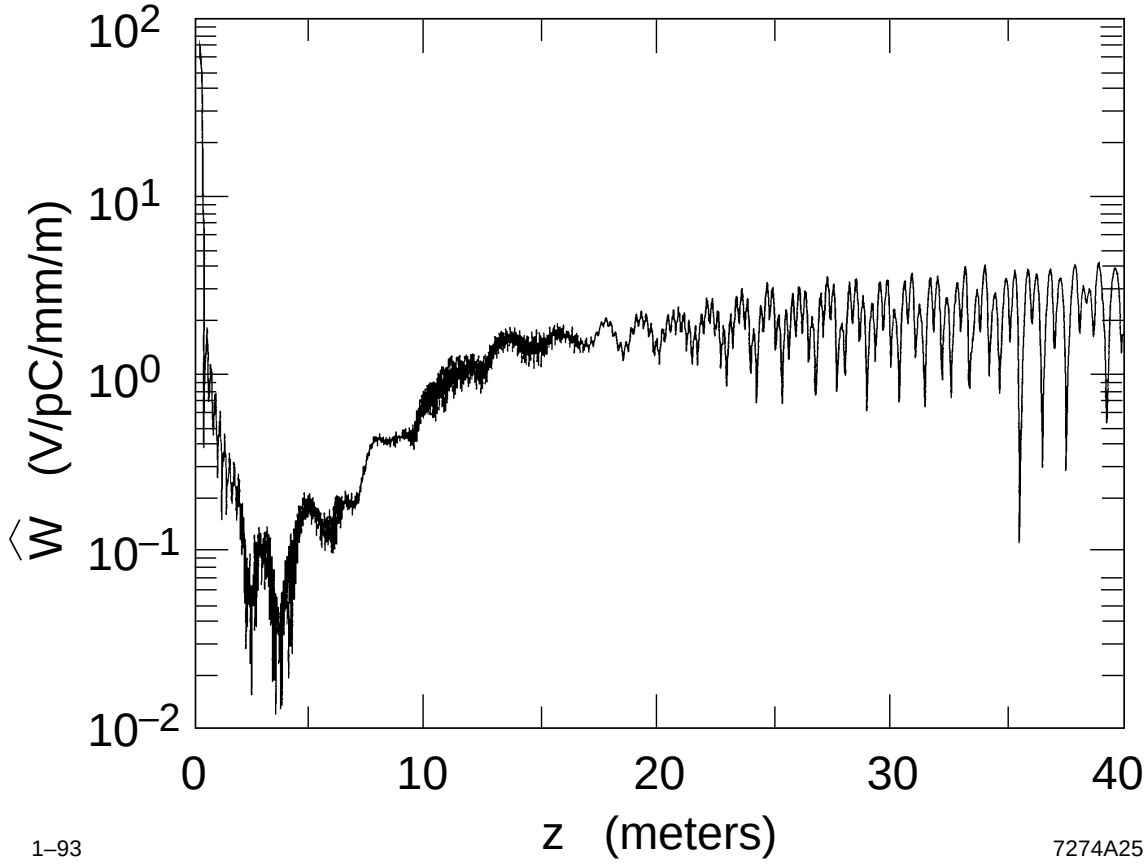

Fig. 22

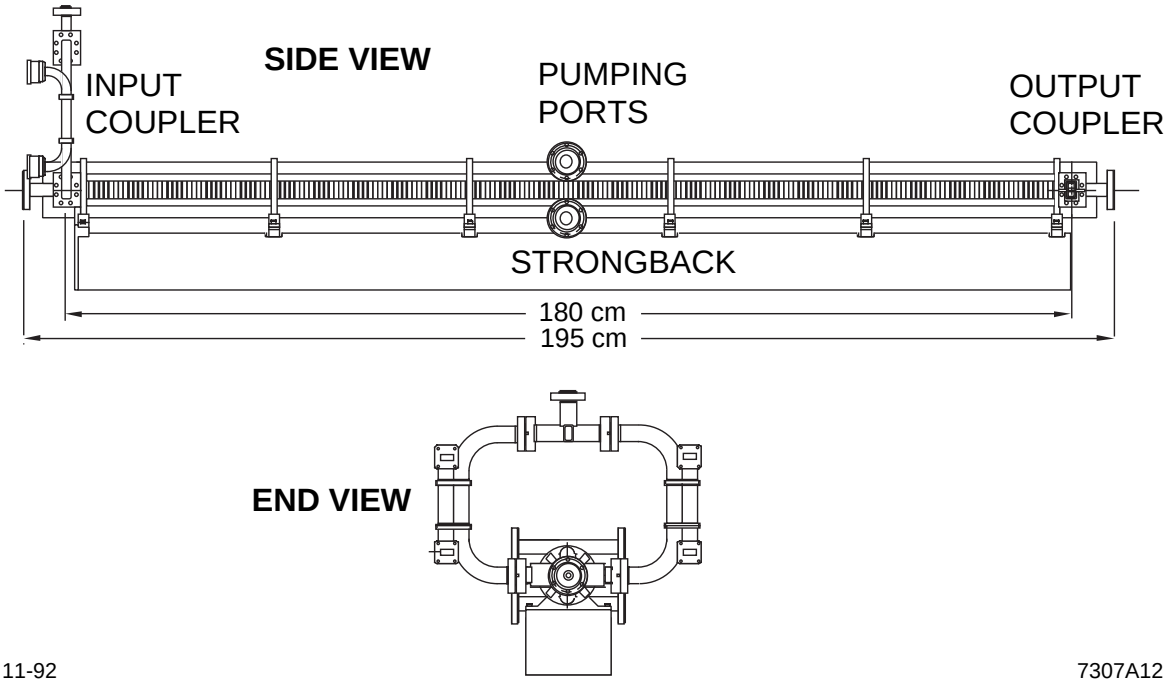
SIDE VIEW
INPUT
COUPLER
PUMPING
PORTS
OUTPUT
COUPLER
STRONGBACK
180 cm
195 cm
END VIEW
11-92
7307A12

Fig. 23

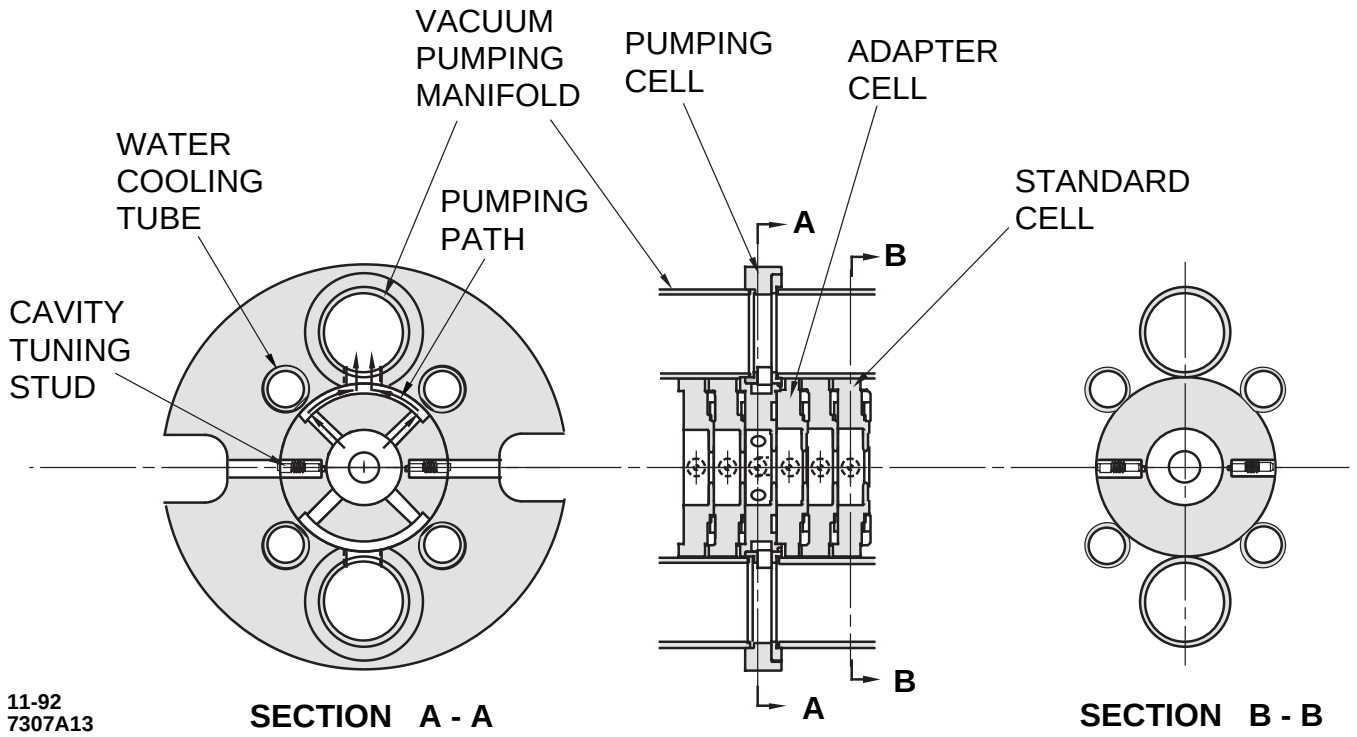
VACUUM
PUMPING
MANIFOLD
PUMPING
CELL
ADAPTER
CELL
WATER
COOLING
TUBE
PUMPING
PATH
STANDARD
CELL
CAVITY
TUNING
STUD
A
B
B
A
11-92
7307A13
SECTION A - A
SECTION B - B

Fig. 24

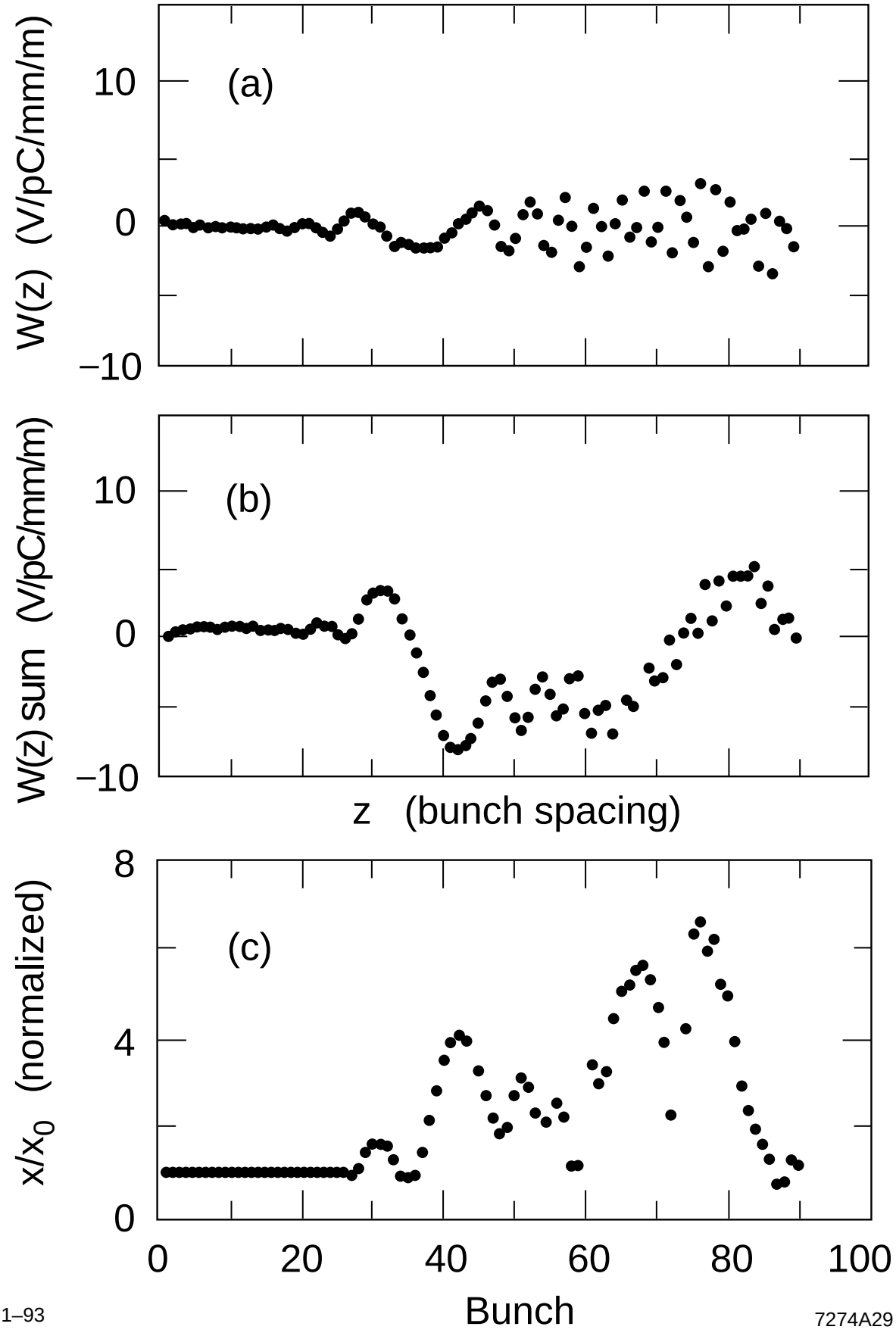
W(z) (V/pC/mm/m)
10
0
−10
(a)
W(z) sum (V/pC/mm/m)
10
0
−10
(b)
z (bunch spacing)
x/x0 (normalized)
8
4
0
(c)
0
20
40
60
80
100
Bunch
1–93
7274A29

Fig. 25

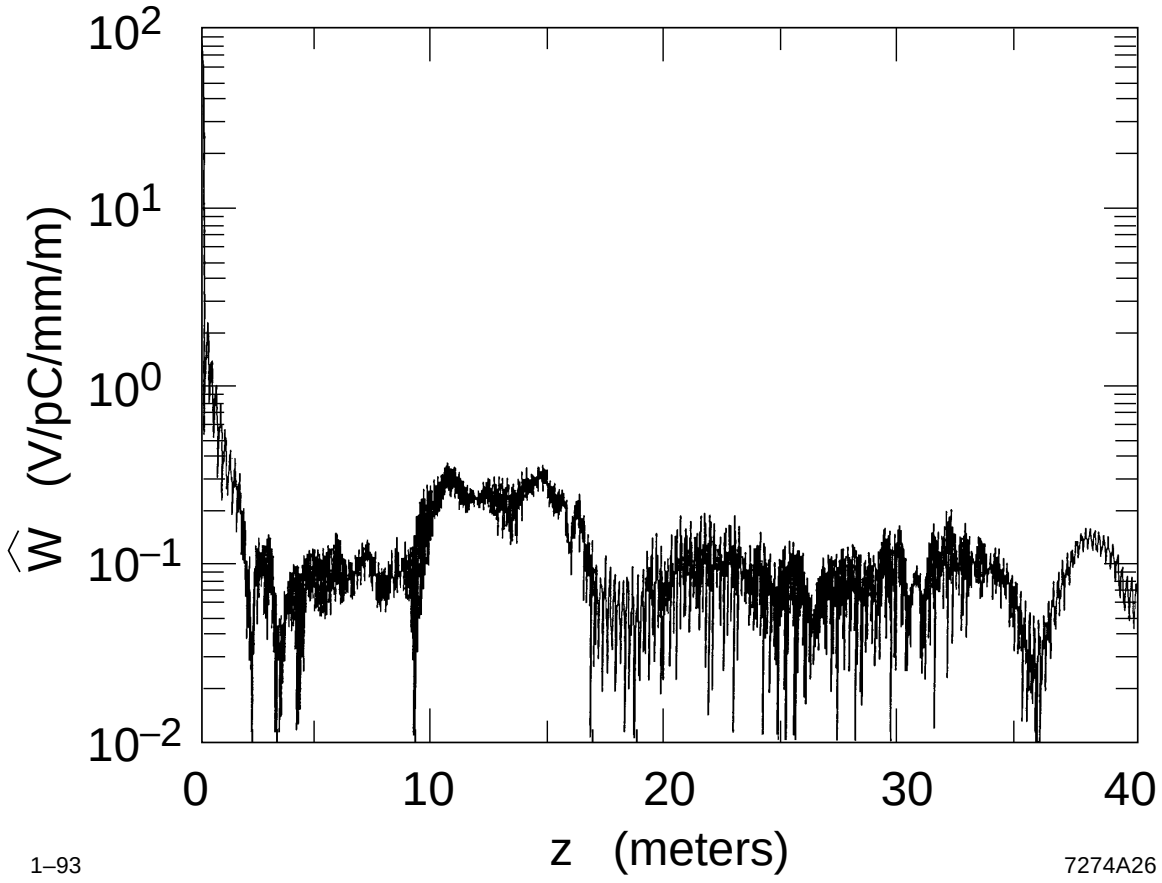
10^2
10^1
10^0
10^{-1}
10^{-2}
$\langle W \rangle$ (V/pC/mm/m)
0
10
20
30
40
z (meters)
1–93
7274A26

Fig. 26

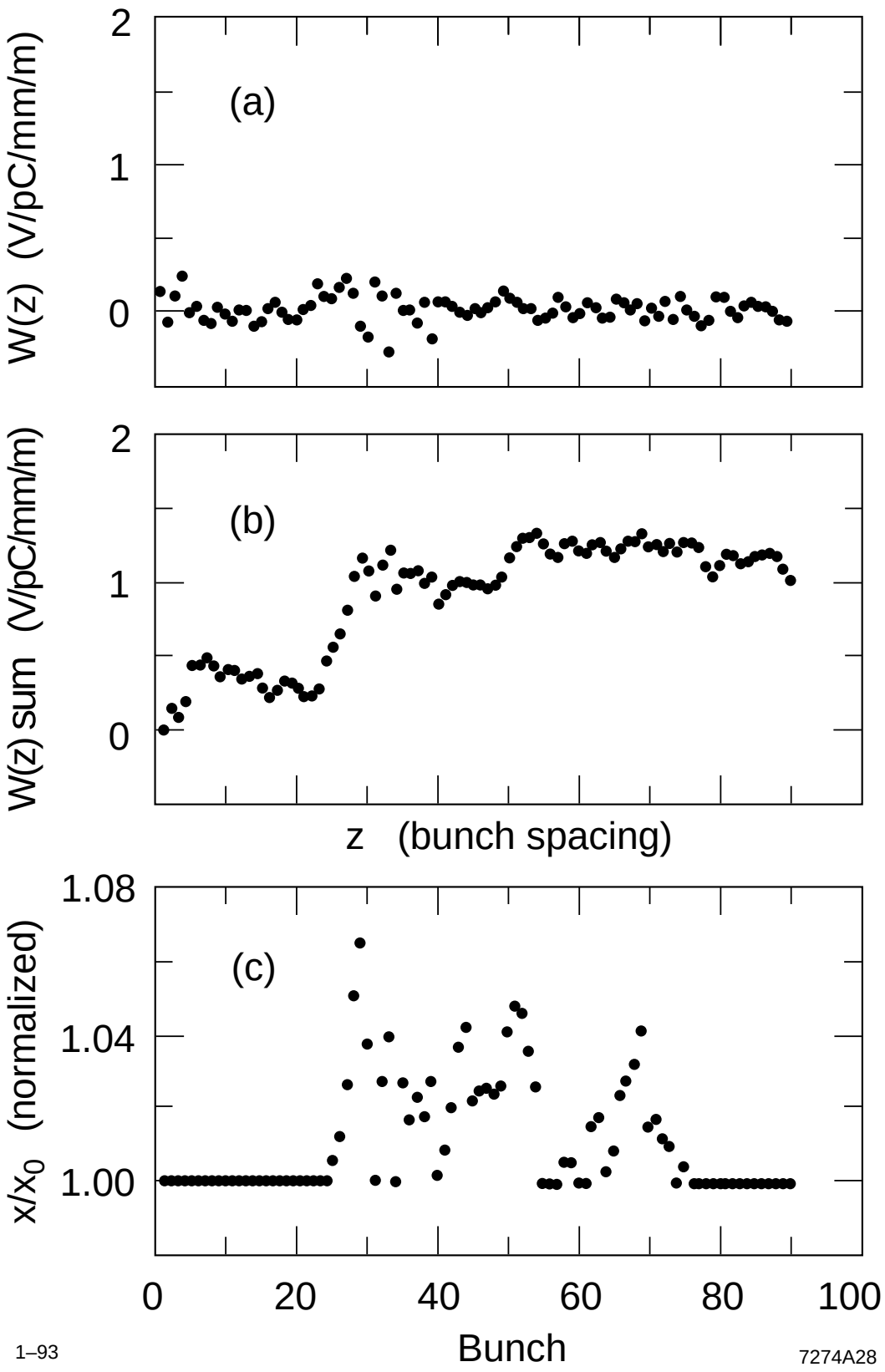
2
1
0
W(z) (V/pC/mm/m)
(a)
2
1
0
W(z) sum (V/pC/mm/m)
(b)
z (bunch spacing)
1.08
1.04
1.00
x/x0 (normalized)
(c)
0
20
40
60
80
100
Bunch
1–93
7274A28

Fig. 27

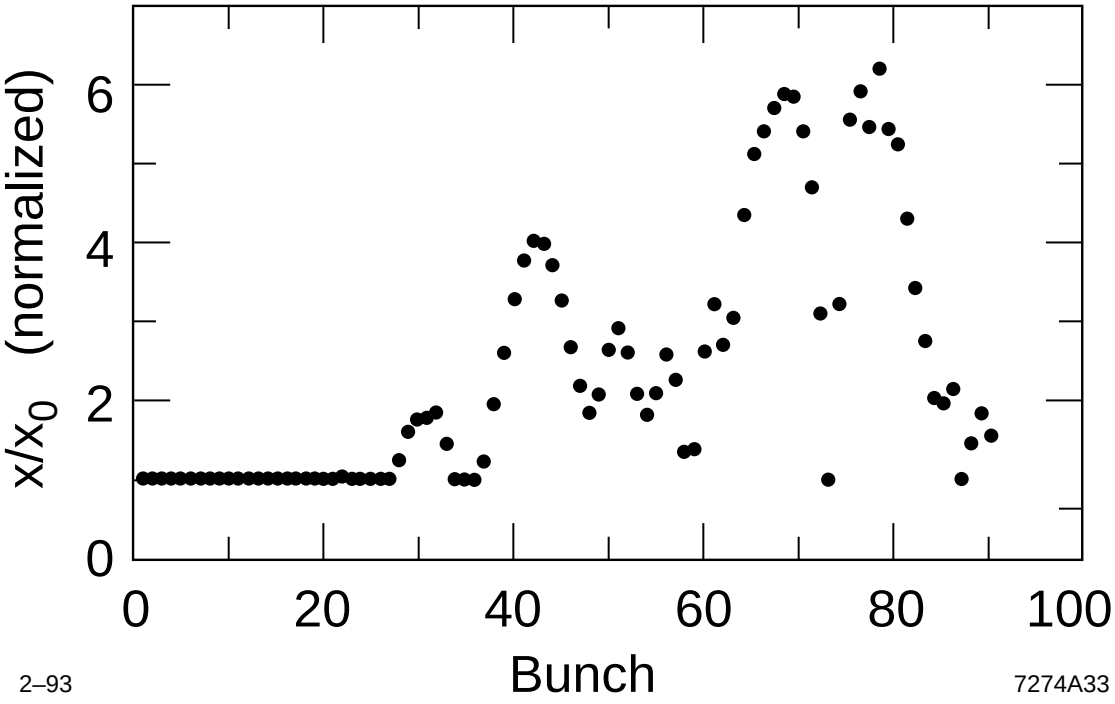

Fig. 28

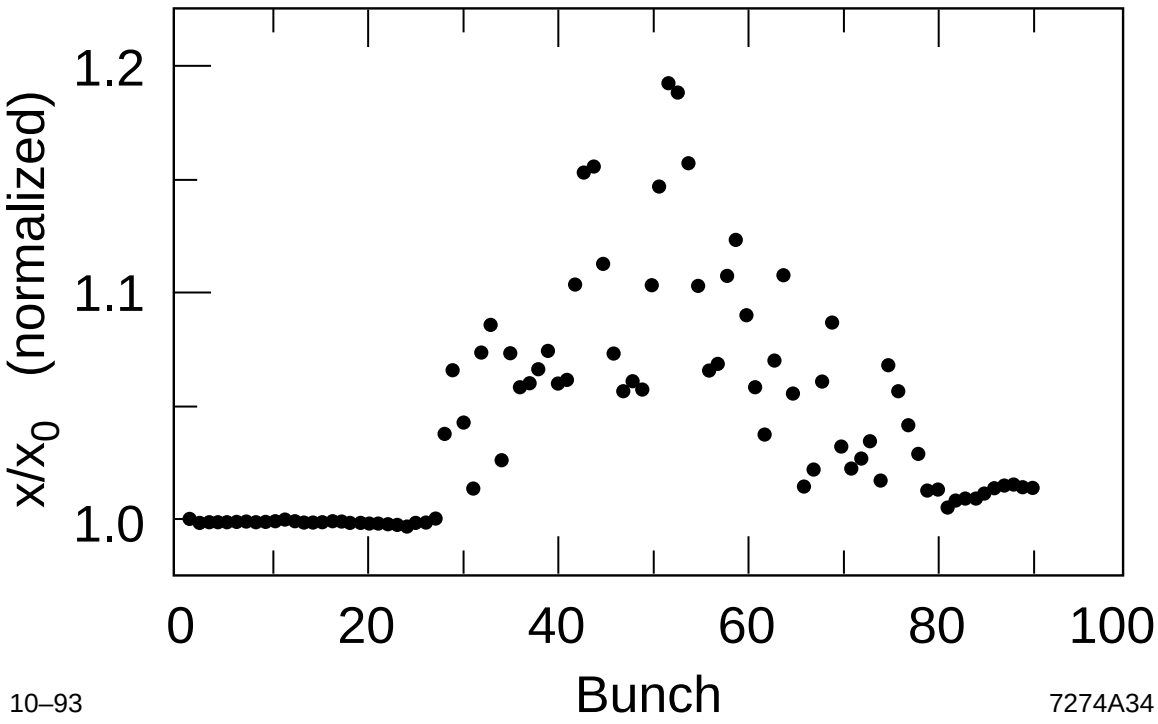

Fig. 29

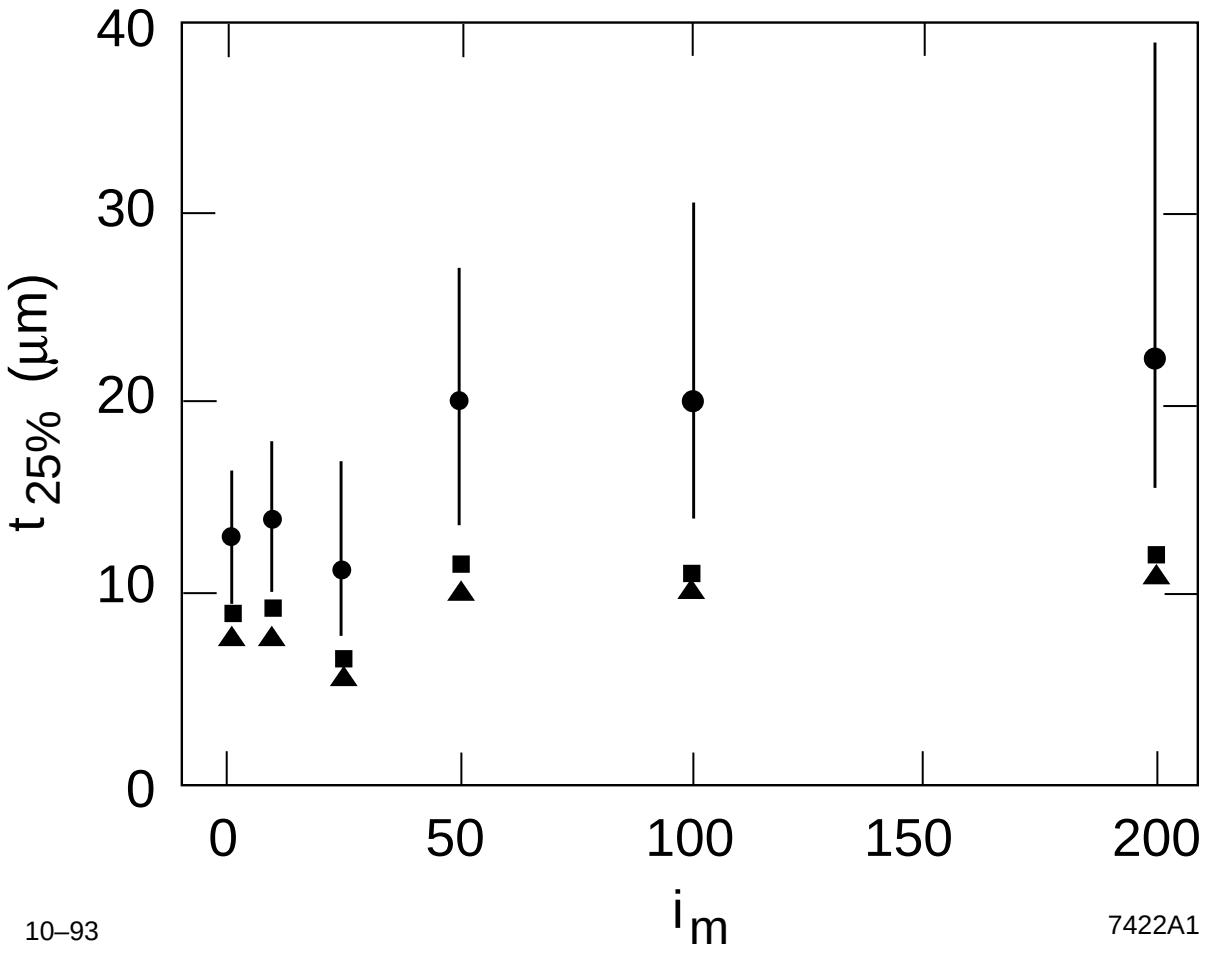

Fig. 30